Optimization and performance analysis of novel waste EPS bead-sand composite cushions for rockfall mitigation: An integrated experimental and numerical study

Hani Meree, Dongpo Wang, Shuaixing Yan, Stéphane Lambert, Yanhao Chen, Qi Dong

Optimization and Performance Analysis of Novel Waste EPS Bead-Sand Composite Cushions for Rockfall Mitigation: An Integrated Experimental and Numerical

Hani Meree[1], Dongpo Wang[1*], Shuaixing Yan[1], Stéphane Lambert[2], Yanhao Chen[1], Qi Dong[1]

[1] State Key Laboratory of Geohazard Prevention and Geoenvironment Protection, Chengdu University of Technology, Chengdu 610059, PR China

[2] Univ. Grenoble Alpes, INRAE, CNRS, IRD, Grenoble INP, IGE, Grenoble, 38000, France

[*] Corresponding author: Dongpo Wang: wangdongpo@cdut.edu.cn

Abstract

This study investigates the optimization of waste Expanded Polystyrene (EPS) bead-sand composite cushions for rockfall mitigation through an integrated approach combining experimental methodologies, statistical optimization, and numerical simulations. Orthogonal Experimental Design (OED) and Response Surface Methodology (RSM) determined an optimal EPS bead content of 38.79% by volume, balancing energy absorption and load distribution. Layered configurations, particularly the SE-S-F (EPS-sand mixture over pure sand) design, outperformed monolithic cushions, achieving a 79.7% reduction in RC slab tension damage compared to traditional sand cushions and a 92.3% reduction in crack width relative to the pure EPS-sand mixture. The SE-S-F configuration also minimized transmitted forces, accelerations, and the energy dissipation factor, while shifting failure mechanisms toward flexural cracking for enhanced structural protection. A validated numerical simulation framework effectively captured impact dynamics, supporting performance predictions. By repurposing waste EPS, this research promotes sustainable construction practices, offering lighter, more effective, and environmentally conscious protection systems with significant implications for safety and cost-efficiency in mountainous regions and transportation corridors.

Keywords: EPS-sand Mixture; Waste material utilization; Orthogonal Experimental Design (OED); Response Surface Methodology (RSM); Layered configuration

1 Introduction

Rockfall, a widespread and destructive hazard in steep, mountainous regions, endangers human settlements, infrastructure, and public safety globally (Loew et al., 2022). Transportation networks, notably roads and railways in these areas, are particularly susceptible to rockfall incidents, which cause casualties, extensive vehicle damage, and considerable economic losses through traffic disruptions and infrastructure failure (Budetta, 2004; Klose et al., 2015; Lan et al., 2010). Climate change exacerbates this risk by intensifying natural disasters (Savi et al., 2021). To counter these threats, engineers and geologists have deployed diverse protective measures, including flexible barriers, check dams, embankments, netting, and rock sheds (Lambert and Bourrier, 2013; Meree et al., 2023b, 2023c; Volkwein et al., 2011). Among these, cushioning systems stand out as essential for absorbing and dissipating the high-impact energy of falling rocks, protecting underlying structures, and prolonging the lifespan of rockfall defenses (Lambert et al., 2009; Su et al., 2019).

Recent advancements in rockfall cushioning systems reflect a drive to improve protection efficacy while addressing environmental and economic constraints. Contemporary research has developed diverse material configurations and composites to optimize energy dissipation and structural integrity under impact loads. Sand-based cushions, valued for their availability, cost-effectiveness, and energy absorption, form a cornerstone of these systems, though efforts to enhance their performance persist. Innovations include soil layers combined with expandable polyethylene (EPE) for flexibility and resilience (Zhao et al., 2018b), geosynthetic-reinforced cohesive soils with enhanced shear strength via geotextiles and geogrids (Hassan et al., 2022), and sustainable stabilization of dispersive clays using potassium-rich waste ash (Hassan et al., 2023a). Multi-layered designs, such as Kishi et al.'s (Kishi et al., 2002) system with EPS, reinforced concrete, and sand, leverage distinct material properties for superior cushioning. Researchers have also explored composites like foam (Kurihashi et al., 2020), rubber-sand mixtures (Chikatamarla, 2007), and repurposed materials including car tires (Sun et al., 2016), aluminum foam panels (Zhao et al., 2018a), and waste tennis balls with sand (Wang et al., 2022), emphasizing sustainability. Flexible systems, such as non-vented airbags with sand (Meree et al., 2023a) and wire-ring net buffers with sand (Jin et al., 2024), adapt to impact forces while ensuring durability. Lightweight Expanded Clay

Aggregate (LECA) in gabion cushions (Meree et al., 2024) further promises cost-effective, sustainable protection along transportation corridors, though optimizing performance across varied impact conditions remains a challenge.

Integrating waste Expanded Polystyrene (EPS) beads into sand-based cushions offers a compelling, sustainable approach to rockfall mitigation. EPS, a lightweight thermoplastic (98% air, 2% raw material by mass), is prized in geotechnical applications for its unique properties (Tamut et al., 2014). First used for pipeline protection in 1988 (Yamada et al., 1989), EPS-soil modification now aids slope stabilization, lightweight embankments, and seismic buffering (Arellano et al., 2011; Bathurst et al., 2007; Stark, 2004), with recent studies showing geosynthetics boosting shear strength and soil behavior across plasticity indices (Hassan et al., 2023b, 2022). In rockfall cushions, EPS beads markedly lighten the system, a key advantage over sand-only designs where load-bearing capacity is limited (Liu et al., 2006),while their cellular structure enhances compressibility and energy absorption (Horvath, 2008). Environmentally, repurposing waste EPS reduces landfill burdens (Gao et al., 2011), and unlike EPS-block geofoam, on-site mixing with sand cuts fabrication and transport costs, enabling tailored density and strength (Liu et al., 2006). This leverages local sand, lowering project costs and ecological impact for effective, lightweight protection. Geotechnically, EPS-sand composites reduce unit weight while often improving strength (Ojuri and Ademola, 2016), suggesting superior energy dissipation and force reduction over traditional cushions. Yet, optimizing these composites for rockfall requires deeper insight into dynamic loading behavior, including EPS-to-sand ratios, bead size effects, and repeated impact response, alongside long-term durability across diverse conditions.

This study presents a novel, rigorous approach to optimizing EPS bead-sand composite cushions for rockfall mitigation, blending methodological precision with practical innovation. Unlike prior work, such as Yan et al. (Yan et al., 2022) and Yu et al. (Yu et al., 2024), who studied fixed sand-EPS foam composites (geofoam and EPE boards), relying on static configurations, or El-Sherbiny et al. (El-Sherbiny et al., 2018), Edinçliler and Özer (Edinçliler and Özer, 2014), and Deshmukh et al. (Deshmukh et al., 2022), who tested EPS-soil mixtures for seismic buffering, fills, or pavements with arbitrary ratios, our method employs a two-stage process.

Combining Orthogonal Experimental Design (OED) and Response Surface Methodology (RSM), we systematically refine EPS-to-sand ratios to boost energy dissipation and reduce impact forces. This departs from trial-and-error designs, capitalizing on EPS beads' on-site mixing and adaptability to irregular volumes, advantages over foam systems limited by off-site fabrication (Liu et al., 2006). Distinctively, we pioneer layered cushion optimization, using advanced statistics to balance compressibility and load distribution. Repurposing waste EPS, our work extends the sustainability focus of Wang et al. (Wang et al., 2022) to meet rockfall-specific demands, setting a new standard for efficient, eco-conscious protection systems with wide geotechnical and hazard mitigation implications.

This paper outlines a structured approach to optimizing EPS-sand composite cushions for rockfall mitigation (Figure 1). The Materials and Methods section characterizes sand-EPS mixtures via geotechnical tests and details the experimental design, including physical modeling, instrumentation, and procedures for Orthogonal Experimental Design (OED), Response Surface Methodology (RSM), and successive impact testing. The Results and Analysis section examines outcomes from these methods, followed by the Numerical Simulation section, which covers methodology, model setup, validation, layered configurations, and comparative analysis. The Discussion synthesizes experimental and numerical insights, addressing implications, limitations, and future research directions. The Conclusion summarizes key findings and their role in advancing rockfall mitigation. This framework integrates material testing, optimization, impact analysis, and modeling to deliver an efficient, sustainable solution for rockfall protection.

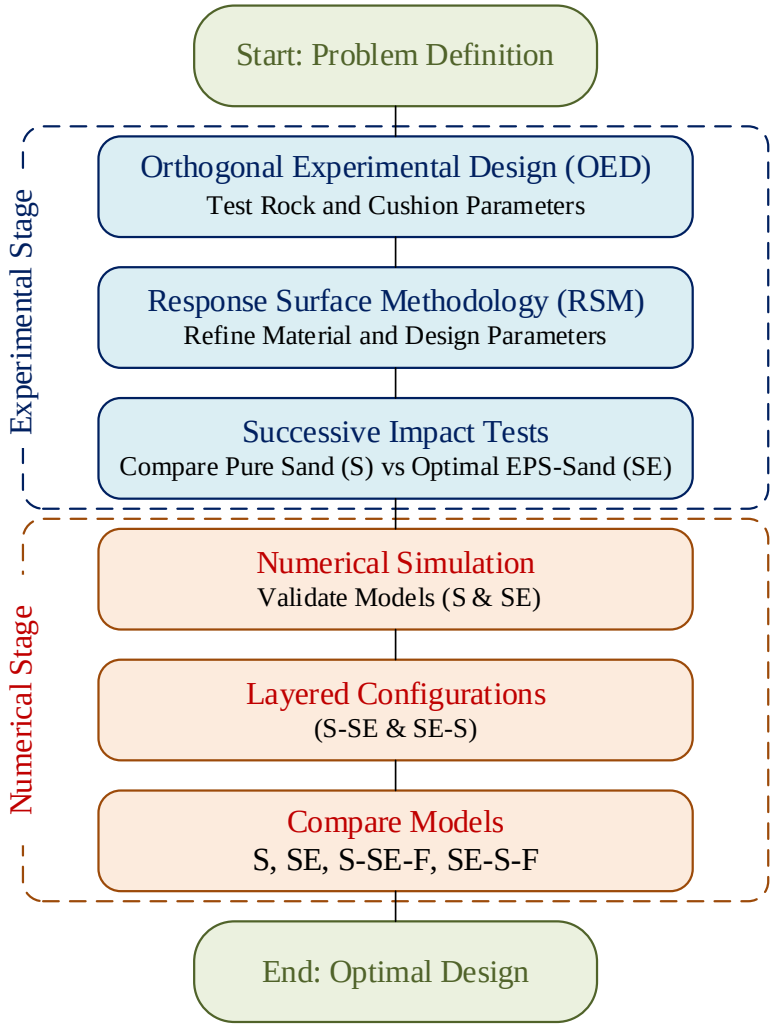

Figure 1 Flowchart of the research methodology for optimizing EPS-sand cushions, integrating experimental and numerical stages

2 Materials and Methods

2.1 Materials

This study used river sand and waste Expanded Polystyrene (EPS) beads to create rockfall cushioning composites. The sand, sourced from Guanghan, Sichuan Province, China, is a natural siliceous material typical in local construction. It was oven-dried at 105°C for 24 hours and sieved through a 4.75 mm Indian Standard (IS) sieve to ensure uniformity. The EPS beads, sourced from Langfang Yutian Environmental Protection Technology

Co., Ltd. in Langfang City, Hebei Province, China, were repurposed from discarded packaging. These white, spherical beads ranged from 3 to 5 mm in diameter.

2.2 Preparation of Sand-EPS Bead Mixtures

To achieve homogeneous sand-EPS bead mixtures, a wet mixing method was employed following El-Sherbiny et al (El-Sherbiny et al., 2018), as initial dry mixing resulted in particle segregation, with the lighter EPS beads separating from the heavier sand. Mixtures were prepared at EPS volumetric ratios of 0% (pure sand), 20%, 35%, and 60%, with water incrementally added to reach the Optimum Moisture Content (OMC) determined from Modified Proctor Tests. This approach enhanced cohesion between EPS beads and sand grains, ensuring consistent material properties across experiments. Each sample was hand-mixed for 5 minutes to achieve visual uniformity, a method selected to minimize damage to the EPS beads while ensuring even distribution. Consistent mixing energy and duration were maintained across all samples to ensure reproducibility. The mixtures were characterized using standard photography (smartphone camera), stereo microscopy (Motic SM7 with MOTICAM PRO S5 PLUS), and Scanning Electron Microscopy (Thermo Fisher Prisma E) to examine the material composition and distribution at the tested volumetric ratios (Figure 2). To quantitatively assess homogeneity, the SEM image at 35% EPS (Figure 2c) was analyzed using ImageJ software. The image was divided into a 5×5 grid, and the percentage of EPS beads in each region was calculated, yielding a mean of 32% with a standard deviation of 3.5%. The resulting Coefficient of Variation (CV) of 10.9% indicates good homogeneity, corroborating the visual evidence of uniform EPS bead distribution within the sand matrix.

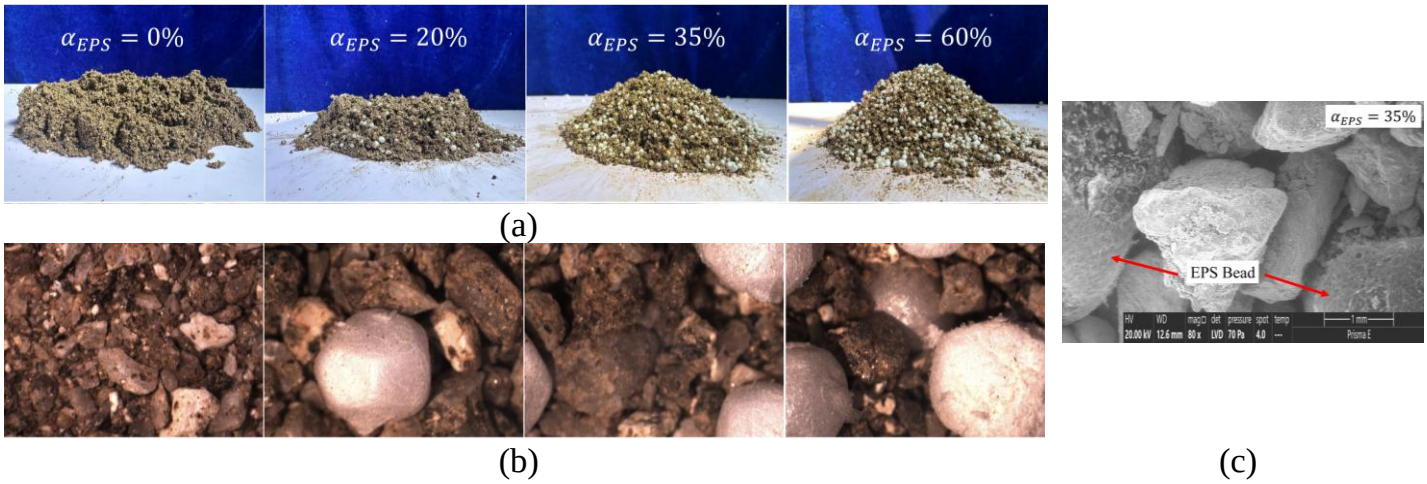

Figure 2 Sand-EPS mixtures at different scales. (a) Standard photographs, (b) Stereo microscope images, and (c) SEM image at 35% EPS.

2.3 Geotechnical Characterization

2.3.1 Modified Proctor Tests

Modified Proctor Tests, conducted per ASTM D1557 (ASTM Committee D-18 on Soil and Rock, 2009), determined the Optimum Moisture Content (OMC) and Maximum Dry Density (MDD) for sand-EPS mixtures at various EPS ratios. Each 3 kg mixture was compacted in a 102 mm diameter, 116 mm height mold in five layers, with each layer receiving 25 blows from a 4.5 kg rammer dropped from 450 mm, delivering 2682 kJ/m³ of impact energy. The Modified Proctor Test was chosen over the Standard Proctor Test (American Society for Testing and Materials, 2021)(~600 kJ/m³) due to its higher compaction energy, better simulating the densification required for sand-EPS composites under dynamic rockfall impact loads. To prevent thermal damage to EPS beads, samples were dried at 70°C in a convection oven instead of the standard 110°C, extending drying time but preserving EPS integrity. Moisture content was monitored by weighing samples hourly until a constant mass was achieved (less than 0.1% mass change over 1 hour), ensuring accurate OMC values without compromising composite properties.

Figure 3 illustrates the geotechnical properties of the mixtures. Figure 3(a) shows the relationship between EPS content (α_{EPS}) and OMC. Pure sand exhibited an OMC of 16.6% and an MDD of 3210 kg/m³. As EPS content increased, OMC peaked at 14.5% for 35% EPS before declining to around 13% at 60% EPS. This non-linear trend

results from the interplay between sand capillarity and EPS-induced porosity, alongside EPS's hydrophobic nature. Stereo microscope and SEM images (Figure 2(b) and 2(c)) corroborate this observation, showing that EPS beads create larger void spaces within the sand matrix. These voids enhance water retention at lower EPS contents (0–35%) but reduce it at higher EPS contents (>35%), as the hydrophobic EPS limits water retention within these voids. For pure sand, water retention is primarily driven by capillarity, where water is held in small pores between sand grains via surface tension, yielding a high OMC. At lower EPS contents (0–35%), EPS-induced porosity increases the void ratio, creating larger voids that enhance water retention beyond the sand's capillary capacity, thus raising OMC to its peak. At higher EPS contents (>35%), these larger voids reduce the effectiveness of sand capillarity, and the hydrophobic nature of EPS further limits water retention, leading to a decrease in OMC. The MDD of the sand-EPS mixture (1860 kg/m³) was notably lower than pure sand, due to EPS's lightweight properties. Figure 3(b) depicts a linear decrease in specific gravity (G_s) with increasing EPS content (α_{EPS}), consistent with EPS's low density. These OMC values were maintained in all experiments to ensure consistency and prevent bead segregation, guaranteeing the homogeneity of sand-EPS mixtures throughout the study.

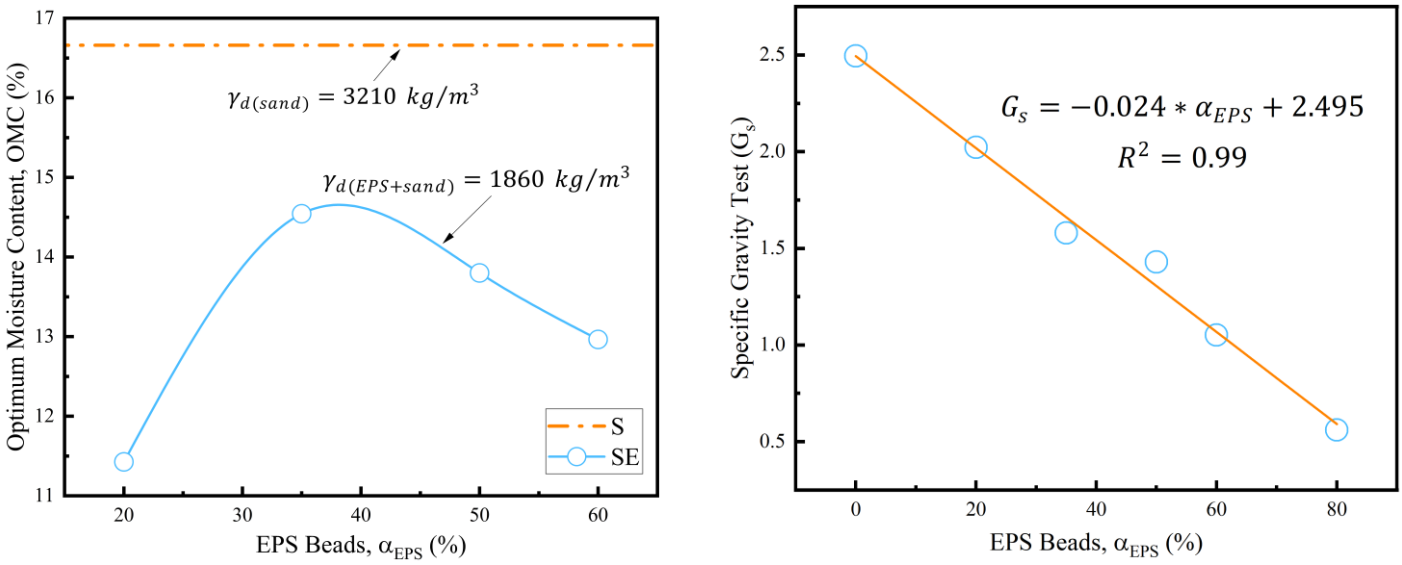

(a) (b)

Figure 3 (a) Relationship between αEPS and OMC, and (b) Relationship between αEPS and Gs

2.3.2 Additional Characterization Tests

Additional tests, including sieve analysis, consolidation, and permeability, were conducted on pure sand (S) and a Sand-EPS mixture (SE) with an optimal EPS ratio to be determined later in this study.

2.3.2.1 Sieve Analysis

Sieve analysis, performed per ASTM C136-06 (ASTM, 2006), determined the particle size distribution of S and SE samples. Figure 4 shows the relationship between sieve size, cumulative weight retained (%), and cumulative passing (%). Gradation was quantified using the Fineness Modulus (FM), Coefficient of Uniformity (C_u), and Coefficient of Curvature (C_c). For pure sand (S), FM, C_u, and C_c were 2.85, 7.63, and 1.14, respectively, while the Sand-EPS mixture (SE) exhibited values of 3.54, 4.25, and 0.94. The higher FM for SE indicates coarser gradation, likely due to EPS beads, while its lower C_u suggests greater uniformity. C_c values near 1.0 for both samples confirm well-graded materials. Figure 4 presents the particle size distribution curves for S and SE.

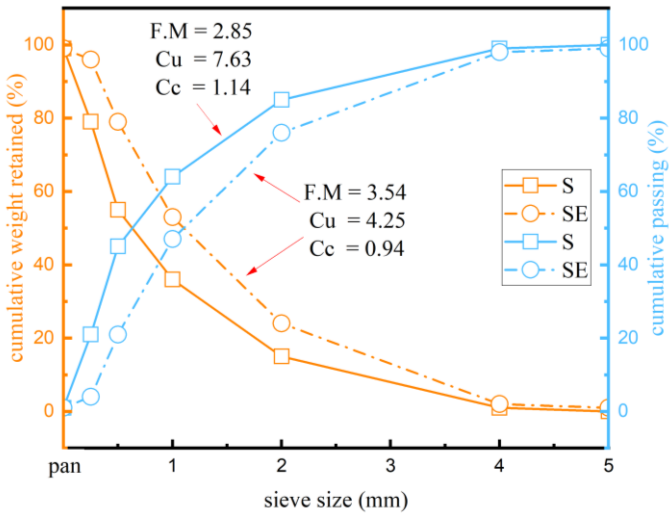

Figure 4 Particle size distribution curves for pure sand (S) and sand-EPS mixture (SE)

2.3.2.2 Consolidation Tests

Consolidation tests, conducted per ASTM D2435 (ASTM Committee D-18 on Soil and Rock, 2011), assessed the compressibility of S and SE samples prepared at their optimum moisture contents from Modified Proctor Tests. Samples were tested in a 61.8 mm diameter, 20 mm height consolidation mold under incremental loads of 50, 100, 200, and 400 kPa, each maintained for 24 hours to ensure complete consolidation. These loads

reflect typical geotechnical stress ranges. Deformation was recorded at 0.1, 0.25, 0.5, 1, 2, 4, 8, and 24 hours per load increment. Figure 5 shows the relationship between applied pressure and void ratio for both samples. Consolidation parameters, compression index (C_c), coefficient of compressibility (a_v), and coefficient of volume compressibility (m_v), were derived. For pure sand (S), C_c, a_v, and m_v were 0.114, 3.42×10^{-4} kPa^{-1}, and 6.02×10^{-5} kPa^{-1}, respectively, while SE showed higher values of 0.199, 5.98×10^{-4} kPa^{-1}, and 7.65×10^{-5} kPa^{-1}. The elevated C_c, a_v, and m_v for SE reflect greater compressibility, attributed to the presence of EPS beads. Stereo microscope and SEM images at 35% EPS (Figure 2(b) and 2(c)) support this finding, showing that EPS beads create larger void spaces and reduce particle-to-particle contact within the sand matrix, allowing greater deformation under load compared to the more densely packed pure sand.

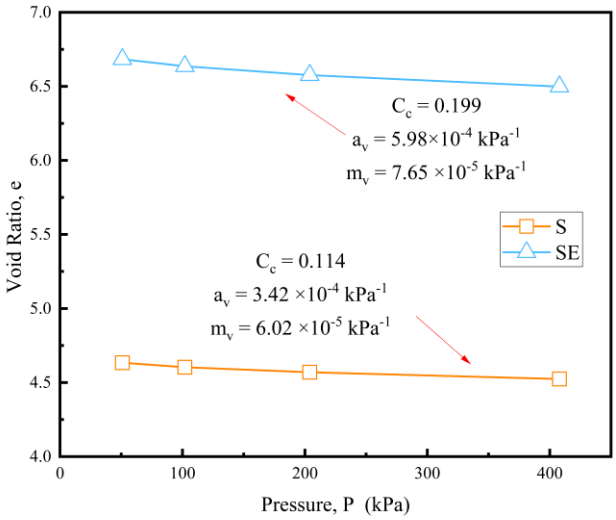

Figure 5 Consolidation curves showing the relationship between applied pressure and void ratio for pure sand and sand-EPS mixture

2.3.2.3 Permeability Tests

Permeability tests, conducted per ASTM D2434 (ASTM Committee D-18 on Soil and Rock, 2006), evaluated the hydraulic conductivity of S and SE samples prepared at their optimum moisture contents. A falling head permeability test was performed using a cylindrical mold (400 mm height, 3000 mm² cross-sectional area) with a standpipe (78.5 mm² cross-sectional area). Samples were saturated by upward water flow, tested at 23 ± 2°C,

and results were corrected to 20°C using viscosity correction factors. Figure 6 illustrates the relationship between water head height and time. The coefficient of permeability at 20°C (K_{20}) was 1.05×10^{-6} m/s for S and 11×10^{-6} m/s for SE, with coefficients of variation below 5% across three replicates per sample. The tenfold higher permeability of SE results from EPS beads creating additional void spaces and flow paths, potentially enhancing drainage and pore water pressure dissipation. This is corroborated by the stereo microscope and SEM images (Figure 2(b) and 2(c)), which reveal a more porous structure in the sand-EPS mixture due to EPS beads, facilitating greater water flow compared to the tighter pore network of pure sand.

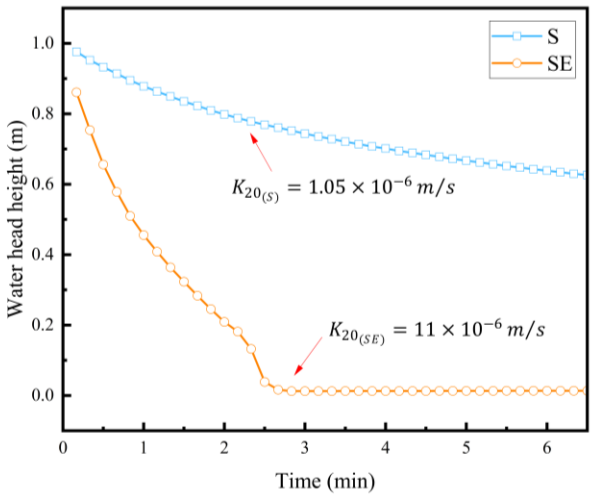

Figure 6 relationship between water head height and time for pure sand and sand-EPS mixture.

2.4 Experimental Design

2.4.1 Physical Model Description

The experimental setup, shown in Figure 7, consists of three main components: a rock block impactor, a reinforced concrete (RC) slab model, and an intervening cushioning layer. Designed to simulate normal impact scenarios, this configuration focuses on the cushioning system's energy absorption and load distribution while excluding oblique collisions. The RC slab, representing a typical rockfall gallery roof, measures 1.5 m × 1.5 m ×

0.2 m and was constructed with C25 grade concrete. It is reinforced with a double-layered HRB335 steel mesh, featuring 20 mm diameter longitudinal bars and 14 mm diameter vertical bars (yield strength: 335 MPa), arranged in an orthogonal grid with 100 mm spacing in both directions to ensure structural integrity under high-impact loads.

To replicate rockfall gallery support conditions, the RC slab was mounted on four C25 concrete pillars (0.2 m × 0.2 m × 0.4 m each). This setup, based on similarity theory with a geometric scale of 7.6, mirrors a real-world rockfall shed, ensuring dynamic similarity in material properties and impact behavior (Wang et al., 2022). In actual rockfall galleries, cushioning materials are confined by side walls to limit lateral deformation. To approximate this in the lab, the cushion layer was constrained within a 1.0 m × 1.0 m central area of the RC slab using a plastic frame, balancing experimental feasibility with real-world relevance. While this setup provides insights into cushioning performance, boundary condition effects on impact response were not the primary focus and thus were not analyzed in detail. The rock block impactor, simulating falling rocks, was designed with varying geometries and weights to study the influence of rock shape and mass on impact dynamics.

Multiple measurement techniques ensured precise data collection. A leveling staff measured the rock block's drop height, maintaining consistent impact energy across tests. A high-speed camera captured the block's motion during impact, enabling analysis of velocity, deceleration, and interaction with the cushion. A white background plate was installed to improve camera footage clarity and enhance motion tracking accuracy. Additionally, a moisture meter periodically monitored the cushion's moisture content, documenting levels that could affect energy absorption and performance.

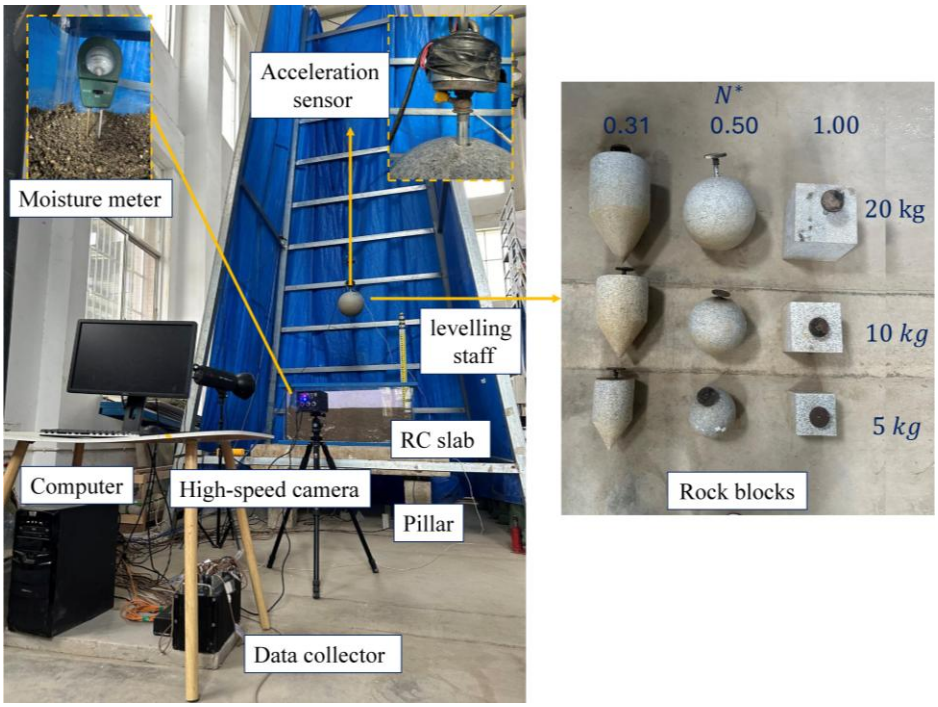

Figure 7 Physical modeling of the test model

2.4.2 Instrumentation and Data Collection

A comprehensive sensor array was deployed to capture the dynamics of the impact event and the structural response of the cushioned RC slab, measuring acceleration, pressure distribution, reaction forces, displacement, and strain. Two accelerometers (AS) were used: one mounted above the falling rock block, connected via an optical fiber cable to minimize signal interference, and another on the central underside of the RC slab to measure transmitted acceleration through the cushion and slab. Pressure distribution was mapped using seven pressure sensors (PS) arranged as shown in Figure 8: one at the cushion's center, three at quarter points, and three at the edges. Strain was monitored with six strain gauges (SG) on the RC slab, three on the top surface and three on the bottom, positioned at the center, edge, and corner as corresponding pairs. Reaction forces at the supports were recorded using four force sensors (FS) placed atop each pillar. Vertical displacement of the slab's center was measured with a laser displacement sensor (DS) positioned on the floor beneath. A calibrated moisture meter periodically monitored the cushion's moisture content to assess its influence on performance.

All sensor data were synchronized and collected using a DHDAS data acquisition system at sampling frequencies of 10 to 100 kHz (Table 1), ensuring capture of rapid impact dynamics. A high-speed camera recorded visual data at 2400 fps, with footage analyzed using Revealer software for motion tracking. Table 1 details the specifications of all instruments, ensuring transparency and reproducibility. All sensors were calibrated per manufacturer specifications before testing to guarantee data accuracy.

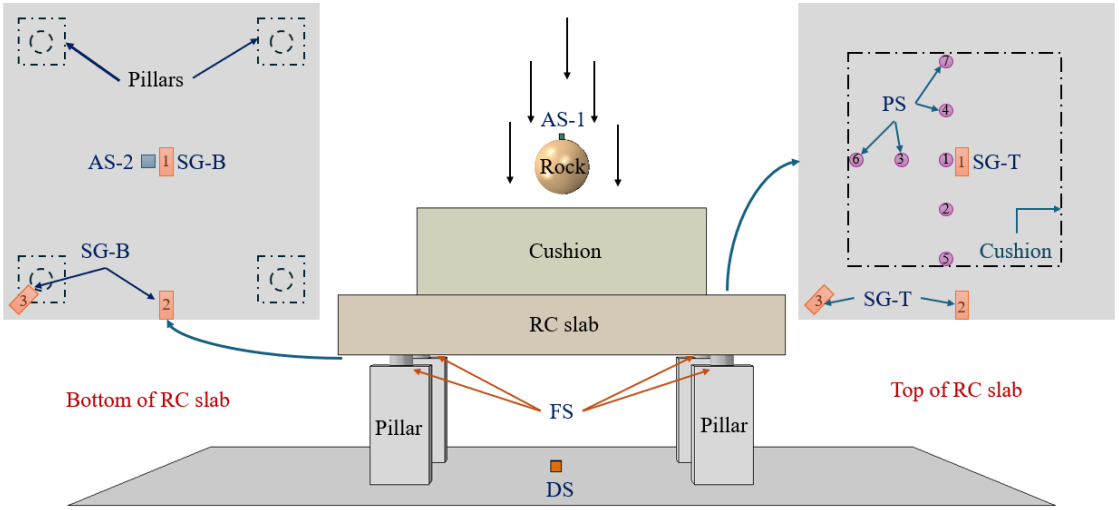

Figure 8 Schematic diagram of the instrumentation layout for the rock impact test on a cushioned RC slab

Table 1 Instruments list in the laboratory experiments

Instrument	Brand	Number	Parameter	Picture
Acceleration sensor	Kistler	2	Measuring range (97.409 - 1014) g, Sensitivity (5.23- 1.01) $\times 10^{-3}$ v/(m/s)^2	
Data collector	Donghua	1	Sampling frequency: 10 - 100 kHz	
Pressure sensors	Zebaisite	7	Measuring range: 3Mpa, Sensitivity 6.52×10^{-7}V/kPa	
Laser displacement sensor	Waycon	1	Measuring range 0.5 m, Sensitivity 20V/m	

Force sensors	Zhongnuo	4	Measuring range100000N, Sensitivity 1.9×10^{-6} V/N	
High-speed camera	Qianyanlang	1	Resolution=2560×1960, FPS=2400, Peak Transfer Rate:65.6G	

2.4.3 Experimental Procedures

2.4.3.1 Orthogonal Experiment Design (OED)

An Orthogonal Experiment Design (OED) was employed to systematically evaluate the influence of multiple factors on the dynamic response of the rock shed, efficiently exploring a multi-dimensional parameter space with minimal trials. Four factors were investigated: cushion thickness (T), rock weight (W), rock block drop height (H), and rock shape factor (N*), each at three levels: T (100 mm, 200 mm, 300 mm), W (5.0 kg, 10 kg, 20 kg), H (1.0 m, 1.5 m, 2.0 m), and N* (0.31, 0.50, 1.00). The rock shape factor (N*), representing conical (0.31), spherical (0.50), and cubic (1.00) geometries, followed Meree et al. (Meree et al., 2024). The waste EPS bead-sand mixture, prepared at a 20:80 volumetric ratio, was selected for its optimal balance of lightweight properties and stiffness, as identified by Edinçliler and Özer (Edinçliler and Özer, 2014), ensuring consistent material properties while isolating the effects of T, W, H, and N*.

A full factorial design would require 81 (3^4) trials, but the orthogonal array L9(3^4) reduced this to 9 experiments while capturing main effects and potential interactions (Table 2). This balanced framework enabled analysis of each factor's relative importance on the rock shed's dynamic response. During each trial, acceleration, impact pressure, and displacement of the rock shed components were measured, providing comprehensive data on system behavior under varied conditions. These results informed subsequent optimization using Response Surface Methodology (RSM), discussed in the next section.

Table 2 Orthogonal Experiment Design Matrix

Experiment	T (mm)	N^*	W (kg)	H (m)

1	100	0.31	5.0	1.0
2	100	0.50	10	1.5
3	100	1.00	20	2.0
4	200	0.31	10	2.0
5	200	0.50	20	1.0
6	200	1.00	5.0	1.5
7	300	0.31	20	1.5
8	300	0.50	5.0	2.0
9	300	1.00	10	1.0

2.4.3.2 Response Surface Methodology (RSM)

Following the Orthogonal Experiment Design (OED), which identified the most influential factors on the rock shed's dynamic response (detailed in the "Results and Analysis" section), Response Surface Methodology (RSM) was employed to optimize the system. RSM enabled a detailed exploration of relationships between key factors and system performance, incorporating the EPS ratio by volume as an additional optimization parameter.

A Central Composite Design (CCD) was selected within the RSM framework for its comprehensive coverage of the experimental space, including corner points, despite being more time-intensive than a Box-Behnken Design (BBD). Three factors were evaluated at three levels: EPS ratio by volume (α_{EPS}: 10%, 35%, 60%), cushion thickness (T: 100 mm, 200 mm, 300 mm), and rock weight (W: 5 kg, 10 kg, 20 kg). Due to laboratory constraints, the midpoint for W was adjusted from 12.5 kg to 10 kg. The rock shape factor (N* = 0.5) and drop height (H = 1.5 m) were held constant at their median values, as OED results indicated their lesser influence on the dynamic response.

The RSM experimental design, detailed in Table 3, comprises 20 runs, including factorial, axial, and center points, to explore main and interaction effects and identify optimal parameter combinations for minimizing the

rock shed's dynamic response. Multiple center points (runs 15–20) assess experimental error and model adequacy. This approach facilitates predictive modeling and response surface analysis to optimize EPS ratio, cushion thickness, and rock weight, enhancing the effectiveness of rockfall mitigation strategies.

Table 3 Response Surface Methodology (RSM) Experimental Design

Run	α_{EPS} (%)	T (mm)	W (kg)	N* (constant)	H (constant)	Point Type
1	10	100	5.0	0.5	1.5	Factorial
2	60	100	5.0	0.5	1.5	Factorial
3	10	300	5.0	0.5	1.5	Factorial
4	60	300	5.0	0.5	1.5	Factorial
5	10	100	20	0.5	1.5	Factorial
6	60	100	20	0.5	1.5	Factorial
7	10	300	20	0.5	1.5	Factorial
8	60	300	20	0.5	1.5	Factorial
9	10	200	10	0.5	1.5	Axial
10	60	200	10	0.5	1.5	Axial
11	35	100	10	0.5	1.5	Axial
12	35	300	10	0.5	1.5	Axial
13	35	200	5.0	0.5	1.5	Axial
14	35	200	20	0.5	1.5	Axial
15	35	200	10	0.5	1.5	Center

16	35	200	10	0.5	1.5	Center
17	35	200	10	0.5	1.5	Center
18	35	200	10	0.5	1.5	Center
19	35	200	10	0.5	1.5	Center
20	35	200	10	0.5	1.5	Center

2.4.3.3 Successive Impact Tests

While the Orthogonal Experiment Design (OED) and Response Surface Methodology (RSM) phases used single impact tests to assess dynamic responses, the final experimental phase evaluated cushion material performance under successive impacts, better simulating real-world rockfall protection scenarios with multiple impacts over time. In the OED and RSM phases, each test configuration was repeated three times for reliability, with additional tests if significant discrepancies arose. After each impact, the cushion's upper surface was restored by removing deformation and compaction effects to ensure consistency.

Following RSM optimization of the EPS bead ratio, a comparative study assessed the optimized Sand-EPS mixture (SE) against traditional sand cushions (S) under successive impacts, mimicking mountain hazard conditions. Each cushion type (SE and S) underwent five consecutive impacts, with no surface remediation or compaction removal between impacts to evaluate cumulative damage and performance degradation. This five-impact sequence was repeated three times per cushion type to ensure reproducibility and account for variability.

Test parameters were held constant: cushion thickness (T) at 200 mm, drop height (H) at 1.5 m, rock block weight (W) at 10 kg, and rock shape factor (N*) at 0.5 (spherical rock). Impacts were spaced 5 minutes apart to allow immediate material recovery. This approach enabled direct comparison of SE and S cushions, assessing

their ability to maintain protective performance over repeated impacts and providing insights into their long-term effectiveness and resilience in rockfall protection systems.

3 Results and Analysis

3.1 Orthogonal Experiment Design (OED) Results

The Orthogonal Experiment Design (OED) systematically evaluated the effects of four factors on the dynamic performance of the EPS bead-sand mixture cushion: cushion thickness (T), rock shape factor (N*), rock weight (W), and drop height (H). This approach efficiently analyzed multiple factors with minimal experimental runs.

Statistical analysis combined Range Analysis and Analysis of Variance (ANOVA) to assess each factor's influence on response variables, using three metrics: range (R), F-value, and P-value. For each factor, the sum of responses at each level (K) was calculated, with the mean (k_i = K / number of levels) providing a normalized measure. The range (R = max(k_i) – min(k_i)) indicated the factor's impact, while the F-value (ratio of between-group to within-group variance) and P-value (from the F-distribution) assessed statistical significance. This method enabled a robust evaluation of each factor's relative importance and significance across response variables.

Results, summarized in Table 4, highlight distinct patterns of factor influence. Cushion thickness (T) was the most influential factor for acceleration responses, showing the highest range (R = 50.37) and significance (F = 3.46, P = 0.10) for rock block acceleration (AS-1), emphasizing its role in energy absorption. Rock weight (W) significantly affected force transmission and strain, with the greatest impact on reaction force (FS: R = 2594, F = 1.56, P = 0.28) and top surface strain (SG-T-1: R = 406, F = 13.64, P = 0.006), indicating a strong link between impact mass and structural response. The rock shape factor (N*) had a lesser influence overall, with its most notable effect on penetration depth (PD: R = 8.13, F = 3.87, P = 0.08), suggesting a limited role in system dynamics despite affecting localized pressure. Drop height (H) showed moderate influence, with its largest effect on AS-1 (R = 32.3, F = 0.66, P = 0.55), indicating that the cushion design can accommodate varying drop heights

effectively. Figure 9 visualizes the contribution ratios, confirming T's dominance in acceleration responses (62% for AS-2, 36% for AS-1) and W's in structural responses (60% for SG-T-1).

Table 4 Statistical analysis results (R, F, P) for each factor and response variable

Response	T (mm)	N*	W (kg)	H (m)
AS-1	(50.37, 3.46, 0.10)	(27.57, 0.46, 0.65)	(30.05, 0.54, 0.61)	(32.3, 0.66, 0.55)
AS-2	(0.006, 21.85, 0.002)	(0.002, 0.26, 0.78)	(0.001, 0.06, 0.94)	(0.001, 0.06, 0.94)
FS	(2153, 1.18, 0.37)	(1725, 0.57, 0.60)	(2594, 1.56, 0.28)	(1996, 0.83, 0.48)
SG-T-1	(182, 0.52, 0.62)	(9.6, 0.001, 1.00)	(406, 13.64, 0.006)	(80.02, 0.10, 0.91)
SG-B-1	(8.15, 1.64, 0.27)	(4.4, 0.34, 0.72)	(8.49, 2.17, 0.20)	(4.76, 0.43, 0.67)
PS-1	(595, 2.98, 0.13)	(347, 0.48, 0.64)	(428, 0.79, 0.50)	(368, 0.55, 0.60)
DS	(0.16, 1.10, 0.39)	(0.14, 0.86, 0.47)	(0.15, 1.05, 0.41)	(0.15, 1.00, 0.42)
PD	(5.87, 1.19, 0.37)	(8.13, 3.87, 0.08)	(3.06, 0.31, 0.75)	(2.71, 0.20, 0.83)

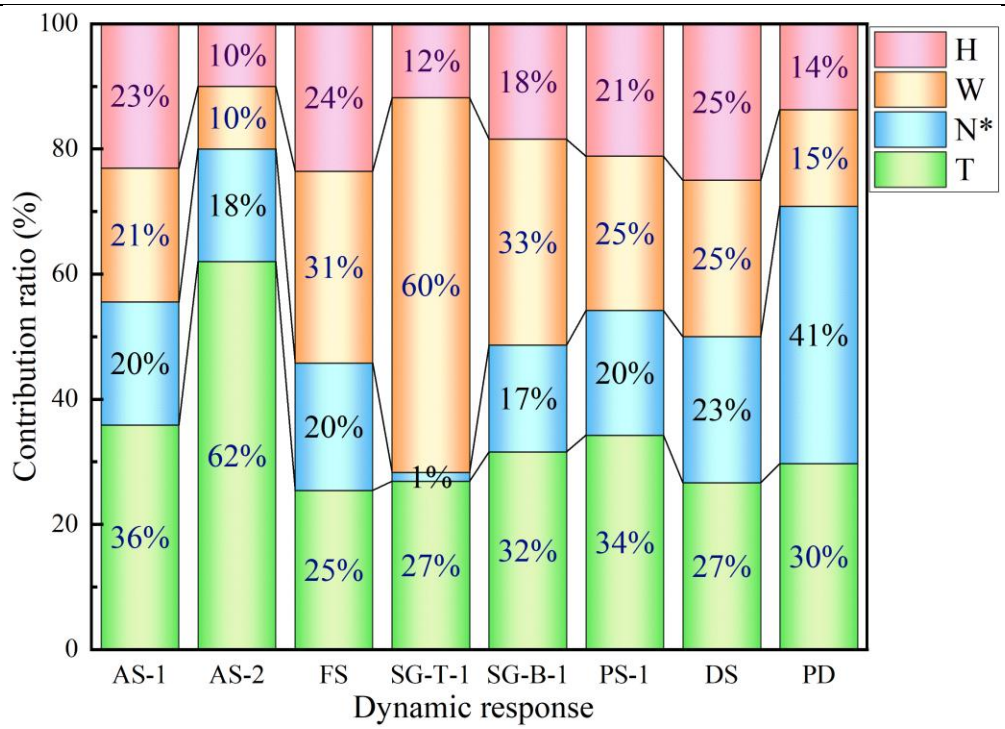

Figure 9 Contribution ratio of factors (T, N, W, H) to different dynamic responses based on OED analysis*

The optimal configuration for minimizing impact forces and accelerations while maximizing energy absorption favors increased cushion thickness (T) and adaptability to varying rock weights (W). Consequently, T and W were selected for further optimization in the Response Surface Methodology (RSM) analysis, which also incorporates the EPS bead ratio, as discussed in the next section.

3.2 Response Surface Methodology (RSM) Analysis

Building on the Orthogonal Experiment Design (OED) findings, which identified cushion thickness (T) and rock weight (W) as key factors influencing the dynamic response, Response Surface Methodology (RSM) was applied to optimize the EPS bead-sand mixture cushion for rockfall mitigation. A Central Composite Design (CCD) was implemented using Minitab software, focusing on EPS ratio (α_{EPS}), cushion thickness (T), and rock weight (W), while holding rock shape factor (N* = 0.50) and drop height (H = 1.5 m) constant to isolate the primary variables' effects.

Model quality was evaluated using the coefficient of determination (R^2) and adjusted R^2 values (Table 5). Most dynamic response models showed high R^2 values (>92%), indicating strong predictive accuracy. However, lower R^2 values for AS-2 (R^2 = 55.33%, R^2(adj) = 15.12%) and DS (R^2 = 69.11%, R^2(adj) = 41.30%) suggest these responses may be influenced by unaccounted factors, requiring further investigation.

Table 5 Model fit statistics for RSM analysis of dynamic response parameters

Metric	AS-1	AS-2	PS-1	FS	SG-T-1	SG-B-1	DS	PD
R-sq (%)	97.75	55.33	96.44	92.40	83.08	94.16	69.11	94.26
R-sq(adj) (%)	95.72	15.12	93.23	85.56	67.86	88.90	41.30	89.10

The RSM analysis highlights the need to balance α_{EPS}, T, and W for optimal performance across dynamic responses. An EPS ratio of 38.79%, with a cushion thickness of 300 mm and rock weight of 8.48 kg, yielded the highest composite desirability (0.91), optimizing all response variables except penetration depth (PD) (Table 6). This optimal α_{EPS} enhances energy absorption through a network of compressible EPS beads within the sand

matrix, while maintaining structural stability. Lower EPS ratios provide insufficient voids for energy dissipation, while higher ratios reduce sand particle contacts needed for load distribution. The 38.79% ratio balances these effects, enabling progressive EPS compression during impact without excessive localized deformation.

Table 6 optimal Factor Settings for Individual and Multiple Response Variables with Composite Desirability

AS-1	AS-2	PS-1	FS	SG-T-1	SG-B-1	DS	PD	α_{EPS}	T	W	Composite Desirability
✓	×	×	×	×	×	×	×	37.27	300.00	5.000	1.000
×	✓	×	×	×	×	×	×	10.00	100.00	16.52	0.720
×	×	✓	×	×	×	×	×	15.05	279.80	20.00	1.000
×	×	×	✓	×	×	×	×	43.33	265.66	5.000	1.000
×	×	×	×	✓	×	×	×	28.69	300.00	7.120	0.990
×	×	×	×	×	✓	×	×	35.76	100.00	5.000	1.000
×	×	×	×	×	×	✓	×	23.64	100.00	5.000	1.000
×	×	×	×	×	×	×	✓	60.00	100.00	10.76	1.000
✓	✓	✓	✓	✓	✓	✓	✓	24.97	174.75	7.270	0.790
✓	✓	✓	✓	✓	✓	✓	×	38.79	300.00	8.480	0.910
✓	×	✓	✓	✓	✓	✓	×	30.71	300.00	6.210	0.997
✓	×	✓	✓	×	✓	✓	×	32.22	300.00	5.000	1.000
✓	×	✓	✓	✓	×	✓	×	30.71	300.00	6.210	0.997

Three-dimensional response surface plots (Figure 10) visualize these relationships, validating the optimal EPS ratio. The left column of Figure 10 shows dynamic responses versus α_{EPS} and T (W fixed at 10 kg), while the right column plots responses versus α_{EPS} and W (T fixed at 200 mm), with N* = 0.5 and H = 1.5 m. Minima in dynamic responses consistently cluster around 37–38% α_{EPS}, aligning with the optimal 38.79% (composite desirability = 0.91). For instance, the left column shows reduced impact effects (e.g., transmitted acceleration,

reaction force) near 37–38% α_{EPS} at higher thicknesses (300 mm), while the right column confirms this trend across rock weights, with minima often at 8–10 kg. This consistency highlights the balance at 38.79% α_{EPS}, where EPS beads enhance energy absorption and the sand matrix ensures load distribution, though slight variations in some responses (e.g., due to lower R^2 for AS-2 and DS) reflect the challenge of uniform optimization across all metrics.

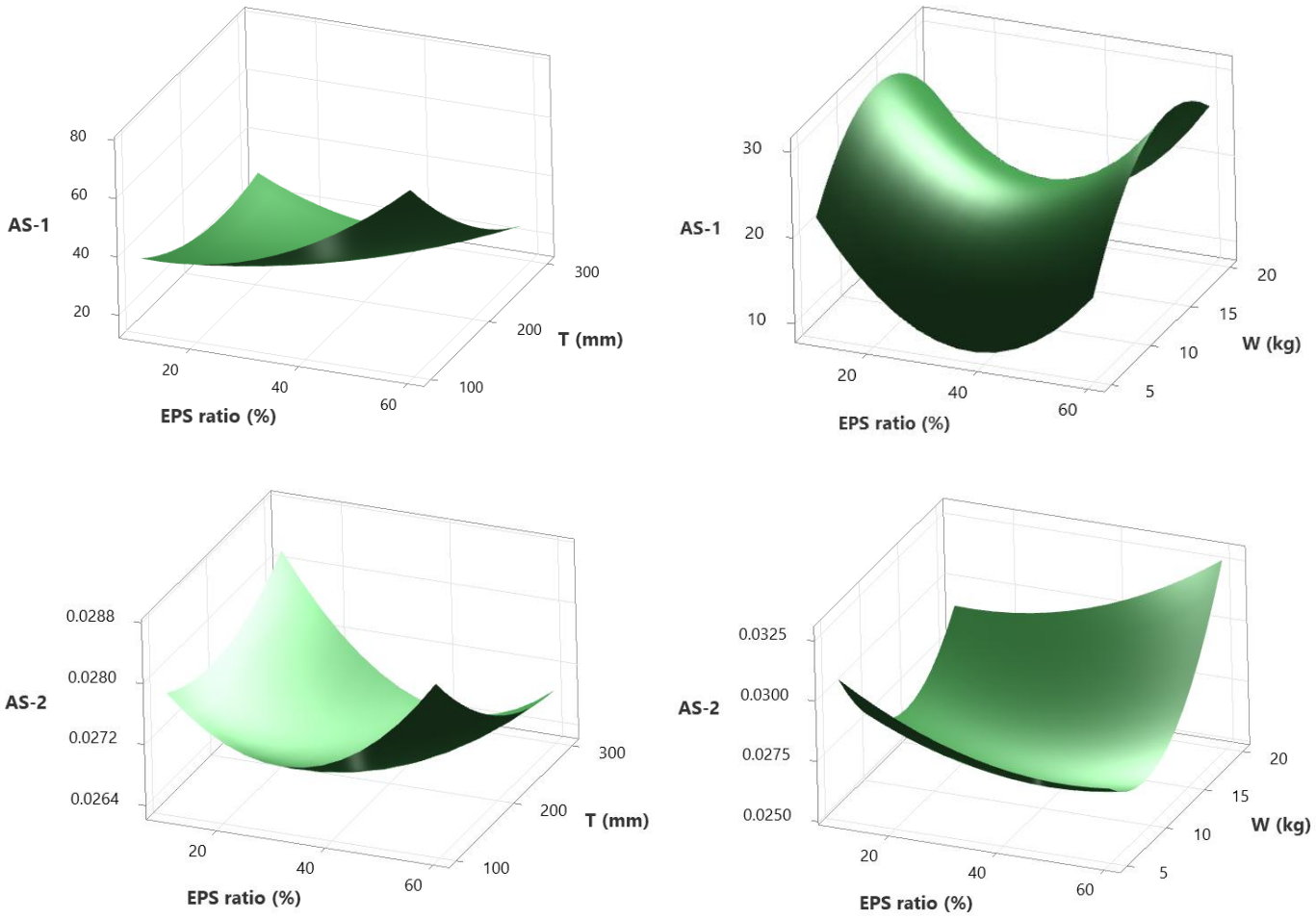

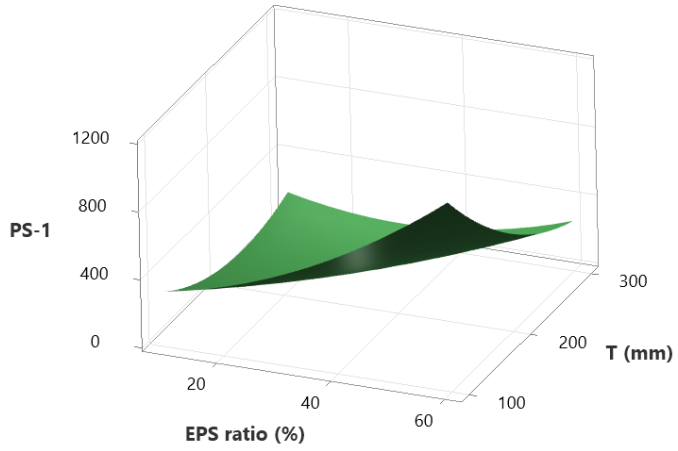
PS-1
1200
800
400
0
20
40
60
EPS ratio (%)
100
200
300
T (mm)

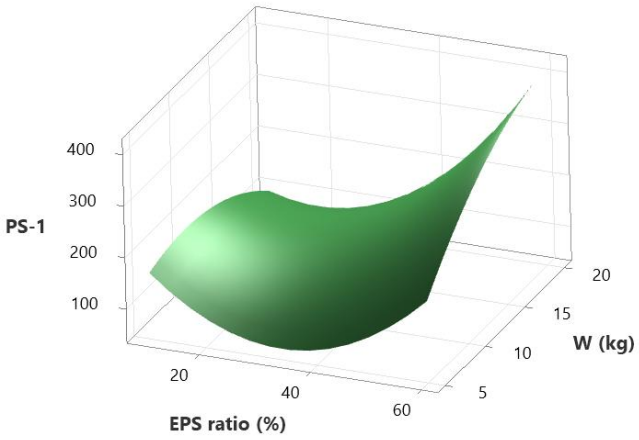
PS-1
400
300
200
100
20
40
60
EPS ratio (%)
5
10
15
20
W (kg)

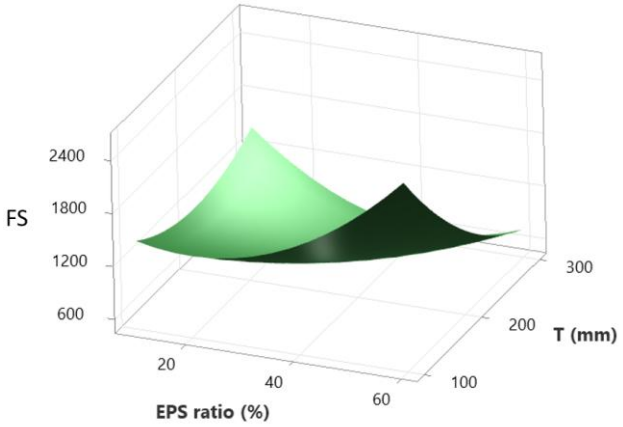
FS
2400
1800
1200
600
20
40
60
EPS ratio (%)
100
200
300
T (mm)

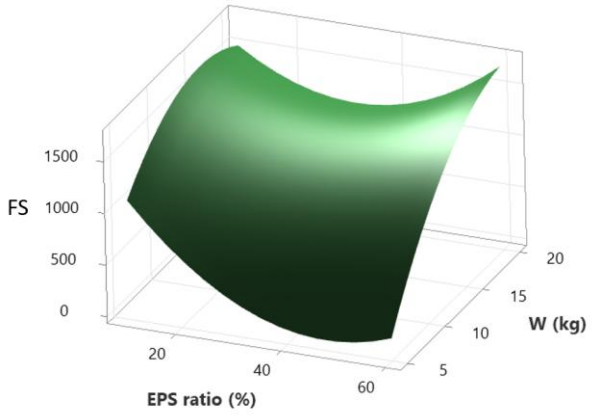
FS
1500
1000
500
0
20
40
60
EPS ratio (%)
5
10
15
20
W (kg)

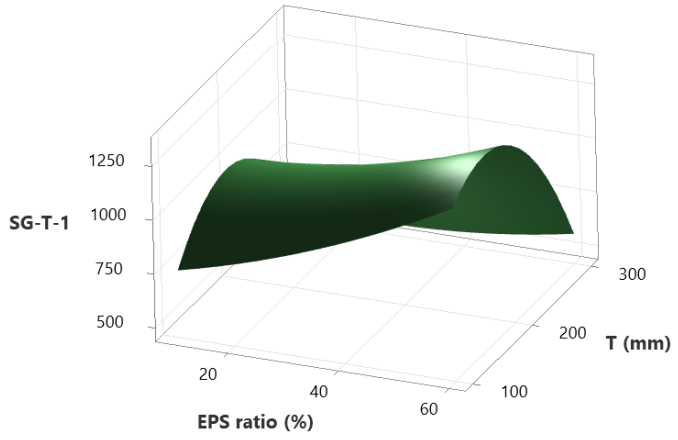
SG-T-1
1250
1000
750
500
20
40
60
EPS ratio (%)
100
200
300
T (mm)

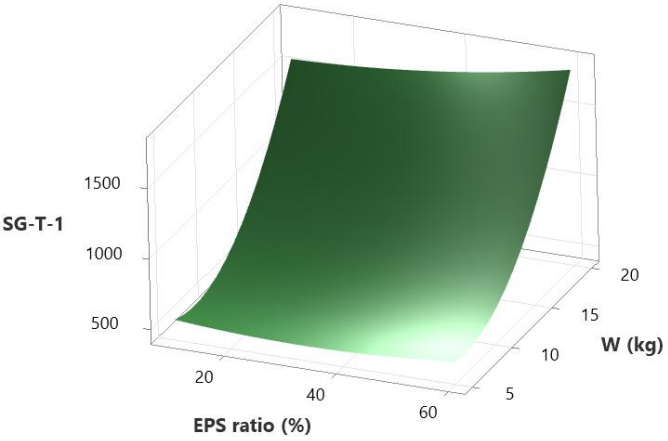
SG-T-1
1500
1000
500
20
40
60
EPS ratio (%)
5
10
15
20
W (kg)

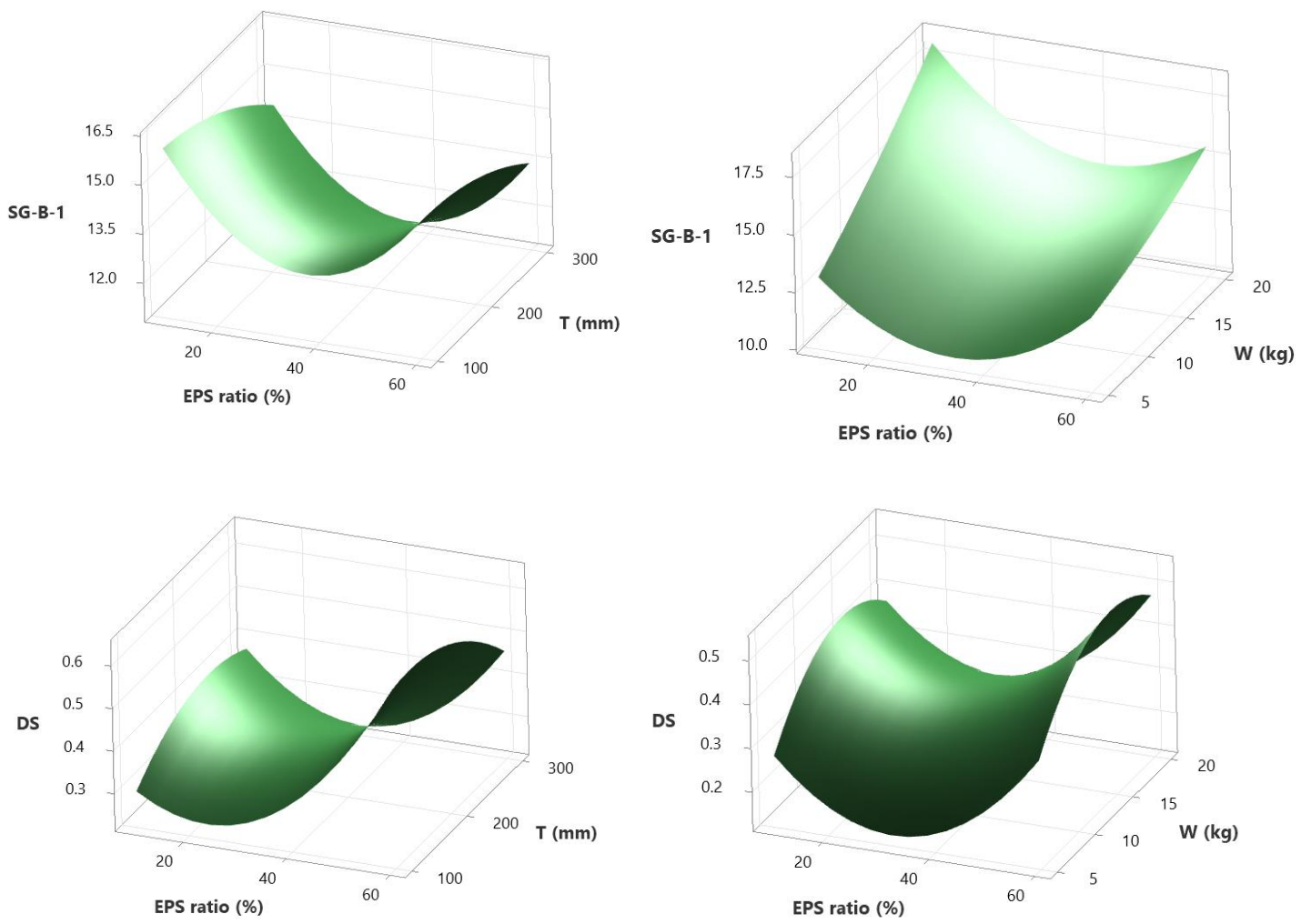

Figure 10 Response surface plots for dynamic response parameters

These findings inform the design of EPS bead-sand mixture cushions for rockfall mitigation. However, limitations in predicting AS-2 and DS responses suggest further research into additional factors or modeling approaches. The potential of layered cushion designs to address these complexities will be explored in subsequent sections.

3.3 Successive Impact Test Results

Successive impact tests were conducted to assess the long-term performance and durability of two cushion materials, pure sand (S) and the sand-optimal EPS ratio mixture (SE), under repetitive loading. Each

sample underwent five consecutive impacts without intermediate adjustments, enabling evaluation of cumulative effects on cushion performance.

Figure 11 compares the dynamic responses of the rock shed structure during the fifth (final) impact, using a dimensionless parameter β, defined as the ratio of the dynamic response of the pure sand cushion (S) to that of the sand-optimal EPS ratio cushion (SE). A β value below 1 indicates better performance by the S cushion, while a value above 1 favors the SE cushion.

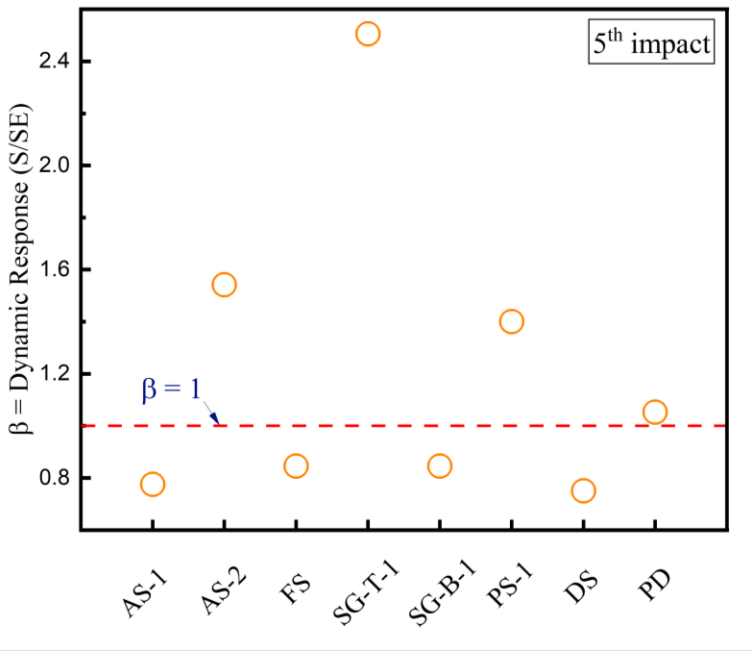

Figure 11 Relationships between β and dynamic response parameters (5th impact)

The results reveal a nuanced performance profile. The SE cushion outperformed the S cushion in acceleration on the bottom surface of the RC slab (AS-2), strain on the upper surface of the slab (SG-T-1), impact pressure under the cushion (PS-1) and penetration depth (PD). Conversely, the S cushion performed better in acceleration on the rock block (AS-1), reaction forces (FS), strain on the bottom surface of the slab (SG-B-1), and displacement of the RC slab (DS). These findings highlight the trade-offs in cushion design and the need for a comprehensive optimization approach that balances multiple performance criteria.

While optimizing the EPS-sand ratio improved certain aspects of cushion performance, it did not yield universal superiority over the pure sand cushion. The complex interplay between material properties, impact parameters, and structural response underscores the need for a more holistic design strategy, prioritizing specific performance criteria based on application and local geological conditions. Optimizing the EPS-sand ratio alone may not suffice for comprehensive performance gains. These insights pave the way for exploring advanced configurations, such as layered or gradient material designs, in the next section, potentially combining the strengths of both S and SE cushions for more effective rockfall protection.

4 Numerical Simulation

Experimental analysis highlighted limitations in the SE cushion's ability to mitigate all dynamic responses of the rock shed under rockfall impact. To overcome these, a numerical approach was employed to refine cushion design and enhance performance under repeated impacts.

4.1 Numerical Methodology

The dynamic response of a rockfall shed system under impulsive loading depends on both the cushion system and the reinforced concrete (RC) structure. While experimental studies offer valuable insights, numerical simulations allow exploration of diverse scenarios using various methodologies.

Initially, a detailed numerical approach was developed to simulate SE cushion behavior, modeling individual EPS beads as discrete sphere elements within a sand matrix represented as a continuous part via the finite element method (FEM). A Python script was created to support this complex integration. However, this method proved computationally intensive, exceeding available resources due to the large number of small elements required. Although the discrete element method (DEM) might seem appropriate, its assumption of rigid particles does not accurately capture EPS bead properties. Consequently, a more practical FEM-based approach was adopted, treating the sand and EPS beads as a single homogeneous material with composite properties. While this simplification reduces granularity, it significantly lowers computational demands, enabling feasible analyses.

Numerical results were validated against experimental data to ensure reliability, balancing computational efficiency with accuracy for a comprehensive study of SE cushion behavior in rockfall protection systems.

4.2 Numerical Model Setup

A comprehensive numerical simulation of rockfall impact on the gallery system was conducted using ABAQUS 2024 (Figure 12). The Drucker-Prager plasticity model was applied for S and SE cushions, while the Concrete Damaged Plasticity (CDP) model was used for concrete components. The rock block, due to its high stiffness relative to the cushions, was modeled as a discrete rigid element. Interactions were simulated using a general contact algorithm with a penalty function and 'Hard' Contact definition. The bond between the concrete slab and steel reinforcement was modeled with a tie constraint, ensuring a perfect bond consistent with reinforced concrete design. Lateral confinement of the cushion layer was achieved by fixing horizontal degrees of freedom along its surrounding surfaces, replicating the experimental plastic frame and real-world boundary conditions, while vertical displacement remained free to allow deformation under impact.

The initial impact velocity (v_0) was calculated as $v_0 = \sqrt{2 * g * H}$, where g is gravitational acceleration and H is the drop height, neglecting rotational velocity and incident impact angle for simplicity. A mesh sensitivity analysis was performed against experimental data, adopting a uniform 20 mm mesh size for the slab, pillars, and cushions, and a finer 10 mm mesh for the rock block to improve contact dynamics accuracy. The Dynamic Explicit Analysis method was used, employing 8-noded linear brick elements (C3D8R) for the slab, pillars, and cushions; 10-node modified quadratic tetrahedrons (C3D10M) for the rock; and 2-node linear beam elements (B31) for steel rebars.

Material properties, derived from laboratory tests, standard values, and iterative calibration, are listed in Table 7. The reinforced concrete slab included two layers of meshed steel bars with 0.2 m spacing in both directions.

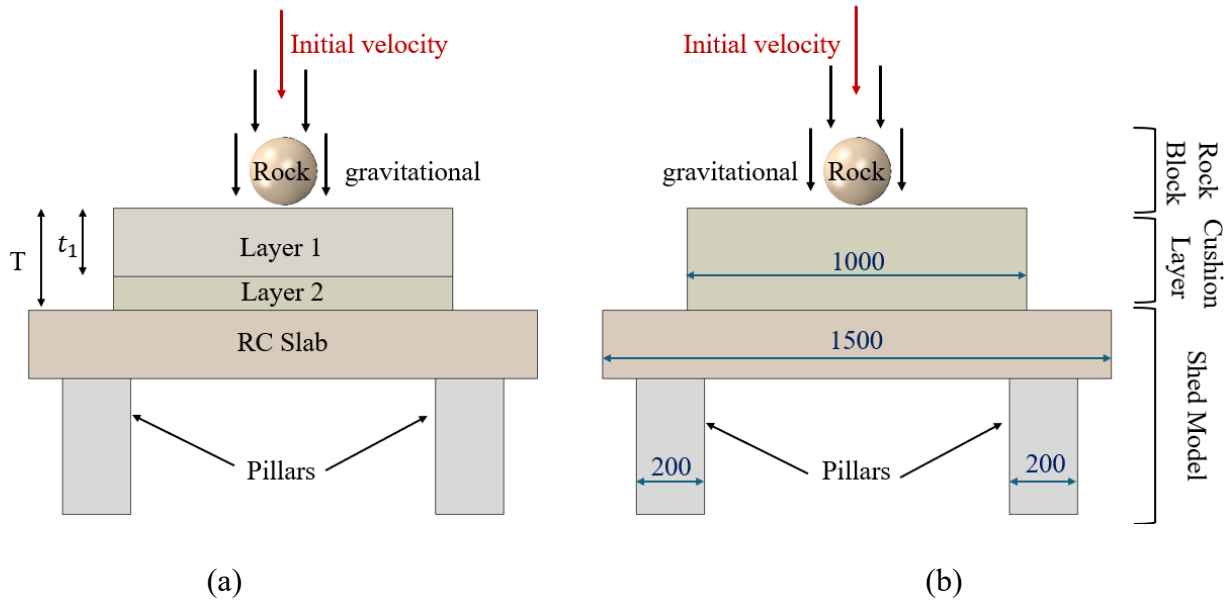

Figure 12 Numerical model configuration (unit: mm)

Table 7 Mechanical Parameters of Materials

Material	Density (kg/m3)	Elastic modulus (MPa)	Poisson's Ratio	Compressive strength (MPa)	Tensile strength (MPa)	Friction angle (°)	Flow Stress Ratio	Dilation angle (°)	Yield stress (MPa)
Concrete	2300	23333	0.2	24.5	2.45	-	-	-	-
Steel	7800	200000	0.27	-	-	-	-	-	461
S	1767	10	0.3	-	-	25	0.778	0	0.1675
SE	1420	30	0.3	-	-	45	0.778	0	0.1675

4.3 Model Validation

The numerical model was validated by comparing its predictions with experimental data, focusing on the temporal response of the rock-cushion system under dynamic excitation. Figure 13 compares the time-varying impact forces for S and SE cushions across five successive impacts. The model accurately captured key experimental observations, including peak magnitudes, duration, and temporal evolution of impact force profiles across different cushion configurations. It effectively reproduced initial force spikes, subsequent oscillations, and

overall force attenuation over time. However, some discrepancies were noted, likely due to the simplification of the EPS-sand mixture as a homogeneous material, idealization of nonlinear and rate-dependent material properties, experimental uncertainties, and simplified boundary conditions. Despite these limitations, the strong overall agreement confirms the model's ability to predict key performance indicators of the rock shed system under rockfall impact scenarios. This validation highlights the complementary role of numerical and experimental methods in understanding rock shed behavior, establishing the model as a reliable tool for further cushion design optimization, including novel layered configurations and material compositions, and enabling performance predictions beyond tested conditions to develop more efficient and robust rockfall protection systems.

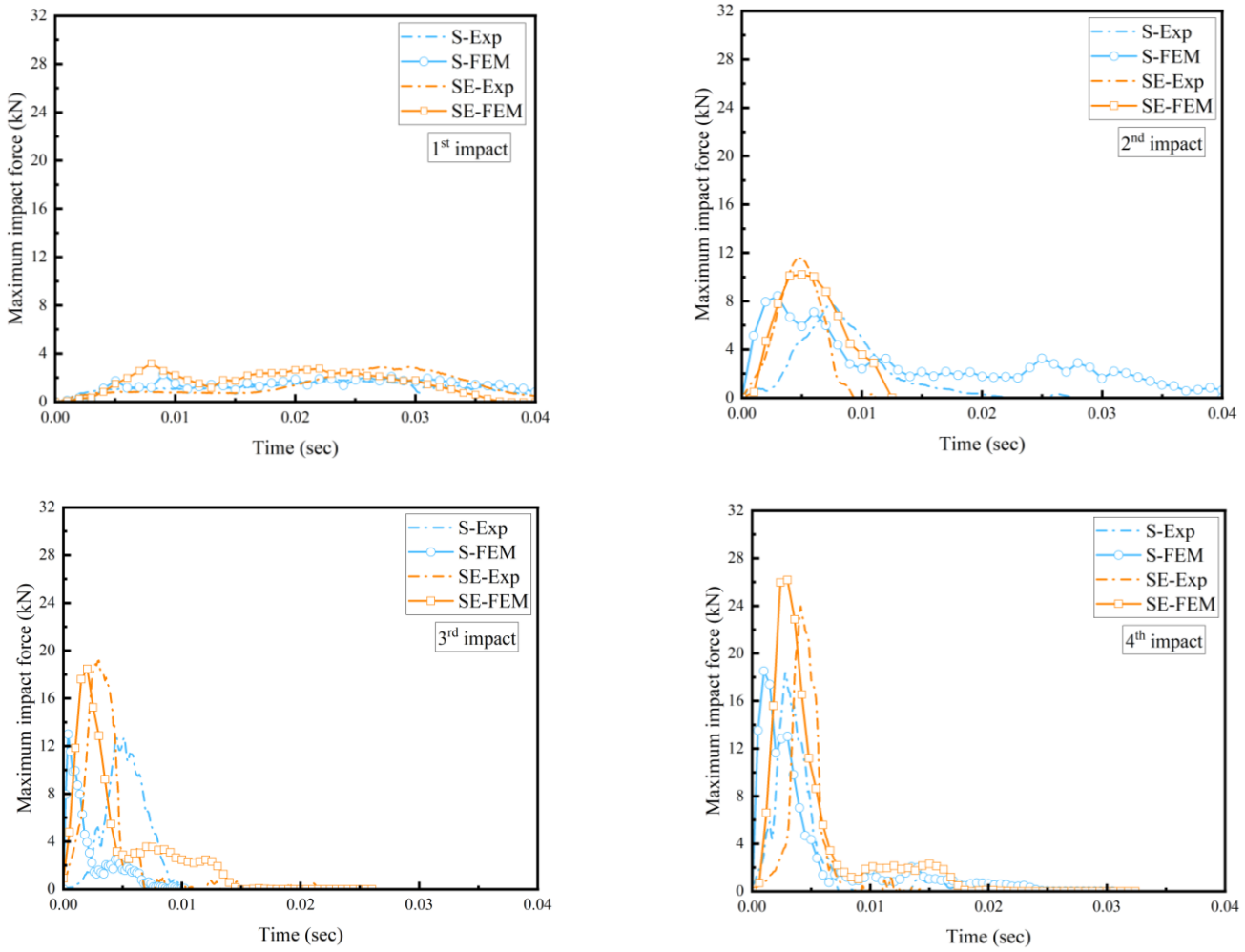

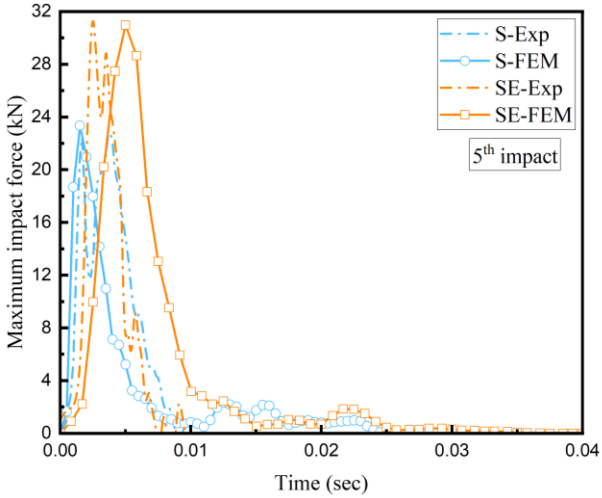

Figure 13 Comparison of experimental and numerical temporal histories of impact force for S and SE cushions

4.4 Proposed Layered Configurations

To address the limitations of the Sand-EPS (SE) cushion in optimizing all dynamic response parameters of the rock shed system compared to the pure Sand (S) cushion, this study proposes two novel layered configurations: Configuration 1 (S-SE), with a sand layer over a Sand-EPS mixture layer, and Configuration 2 (SE-S), with the Sand-EPS mixture as the upper layer (Figure 12(a)). These designs aim to combine the strengths of both materials. For comparison, two monolithic cushions (S and SE) are also analyzed. Using ABAQUS finite element software, these configurations were simulated under five successive impacts, with impact energy increased from 0.2 kJ to 5 kJ to induce and assess damage in the reinforced concrete slab, pushing the system to its limits.

The primary goal is to optimize the thickness ratio of each layer in the layered configurations. A dimensionless factor λ, defined as the ratio of the upper layer thickness to the total cushion thickness ($\lambda = t_1/T$), was introduced. Input parameters include total cushion thickness (T) and λ ratio. Dynamic responses evaluated include impact force on the rock block (F_1), transmitted force under the cushion (F_2), reaction force (FS), penetration depth (PD), vertical displacement of the RC slab at its midpoint (DS), acceleration at the midpoint of the slab's bottom surface (AS-2), and the Global Tension Damage Index (Ψ), which averages the maximum

tension damage parameter (d_t) across all concrete slab elements. These parameters provide a comprehensive assessment of cushion performance and its impact on the underlying structure.

Response Surface Methodology (RSM) with a Central Composite Design (CCD) was employed to determine the optimal λ ratio for each configuration. Table 8 details the experimental design matrix, comprising 13 test runs for each configuration (S-SE and SE-S), with λ ranging from 0.2 to 0.8 and T from 100 mm to 300 mm. This approach enables thorough exploration of the design space to identify optimal layer thickness ratios that enhance the performance of layered cushion systems under successive high-energy impacts.

Table 8 Experimental Design Matrix for Layered Configurations (S-SE and SE-S)

Run	Ratio (λ)	Thickness (mm)	Point Type
1	0.20	100.00	Factorial
2	0.80	100.00	Factorial
3	0.20	300.00	Factorial
4	0.80	300.00	Factorial
5	0.08	200.00	Axial
6	0.92	200.00	Axial
7	0.50	58.580	Axial
8	0.50	341.42	Axial
9	0.50	200.00	Center
10	0.50	200.00	Center
11	0.50	200.00	Center

12	0.50	200.00	Center
13	0.50	200.00	Center

This investigation aims to overcome the limitations of monolithic cushions, developing a more robust and efficient rockfall protection system. The results are expected to provide insights into the interactions between layered materials in impact absorption and force transmission, potentially advancing rock shed design and performance optimization.

4.5 Simulation Results and Analysis

The performance of the Response Surface Methodology (RSM) models for the S-SE and SE-S layered configurations was assessed using coefficient of determination (R^2) and adjusted R^2 values (Table 9). Both configurations showed varying predictive power across dynamic responses. High R^2 values for several responses (e.g., S-SE: F1 at 97.32%, Ψ at 97.54%; SE-S: Ψ at 99.53%, PD at 97.41%) indicate robust predictive capabilities and strong correlations between input factors and key dynamic responses, providing a reliable basis for optimization. However, lower R^2 values for some responses (e.g., S-SE: F2 at 64.79%; SE-S: AS-2 at 62.99%) suggest unaccounted factors in the simplified simulation methodology, highlighting areas for future refinement. This variation underscores the complexity of rockfall impact dynamics and the need for a nuanced approach to cushion design, balancing different dynamic responses and layer configurations.

Table 9 Model Fit Statistics for RSM Analysis of Dynamic Responses in S-SE and SE-S Configurations

Metric	Configuration	F1	F2	FS	PD	DS	AS-2	Ψ
R-sq (%)	S-SE	97.32	64.79	81.73	96.45	76.36	89.14	97.54
R-sq(adj) (%)		95.41	39.65	68.68	93.91	59.47	81.38	95.78
R-sq (%)	SE-S	94.14	82.63	68.73	97.41	90.47	62.99	99.53
R-sq(adj) (%)		89.96	70.23	46.40	95.55	83.66	36.55	99.19

RSM analysis emphasized the importance of balancing the λ ratio and cushion thickness (T) to optimize performance across multiple dynamic responses. Table 10 lists optimal factor settings for individual and multiple response variables, along with composite desirability. For S-SE, the optimal λ ratio was 0.92 with T = 341.42 mm, achieving a composite desirability of 1.00, excelling in responses critical to RC structure integrity (FS, DS, AS-2, Ψ). For SE-S, the optimal λ ratio was 0.63 with T = 341.42 mm, yielding a composite desirability of 0.97, with strong performance in FS and Ψ but less optimization for AS-2 and DS. The analysis prioritized RC structure responses over cushion forces, reflecting the critical role of structural integrity in rockfall mitigation.

Table 10 Optimal Factor Settings and Composite Desirability for S-SE and SE-S Configurations

Configuration	F1	F2	FS	PD	DS	AS-2	Ψ	λ	T	Composite Desirability
S-SE	✓	×	×	×	×	×	×	0.84	287.14	1.00
	×	✓	×	×	×	×	×	0.08	252.85	1.00
	×	×	✓	×	×	×	×	0.92	341.42	1.00
	×	×	×	✓	×	×	×	0.08	58.580	0.96
	×	×	×	×	✓	×	×	0.92	307.14	1.00
	×	×	×	×	×	✓	×	0.92	307.14	1.00
	×	×	×	×	×	×	✓	0.92	335.71	1.00
	×	×	✓	×	✓	✓	✓	0.92	341.42	1.00
	×	×	×	×	✓	×	✓	0.92	332.85	1.00
SE-S	✓	×	×	×	×	×	×	0.38	264.23	1.00
	×	✓	×	×	×	×	×	0.08	198.57	0.94
	×	×	✓	×	×	×	×	0.56	341.42	1.00
	×	×	×	✓	×	×	×	0.08	58.580	0.99
	×	×	×	×	✓	×	×	0.92	341.42	1.00
	×	×	×	×	×	✓	×	0.08	341.42	1.00

×	×	×	×	×	×	✓	0.45	267.14	1.00
×	×	✓	×	✓	✓	✓	0.63	341.42	0.97
×	×	×	×	✓	×	✓	0.67	271.16	1.00

Figure 14 presents optimization plots for S-SE and SE-S, showing Ψ, AS-2, DS, and FS versus λ and T from the RSM analysis. For S-SE, all responses minimize at λ = 0.92 and T = 341.42 mm (D = 1.00), indicating that a thicker cushion effectively reduces dynamic responses. For SE-S, Ψ and FS minimize at λ = 0.63 and T = 341.42 mm (D = 0.97), reflecting improved energy dissipation and force reduction, though AS-2 and DS do not minimize at this point, indicating less optimization for acceleration and displacement. S-SE consistently ties lower responses to increased thickness, while SE-S optimizes Ψ and FS at a moderate λ, highlighting distinct strengths in managing impact effects.

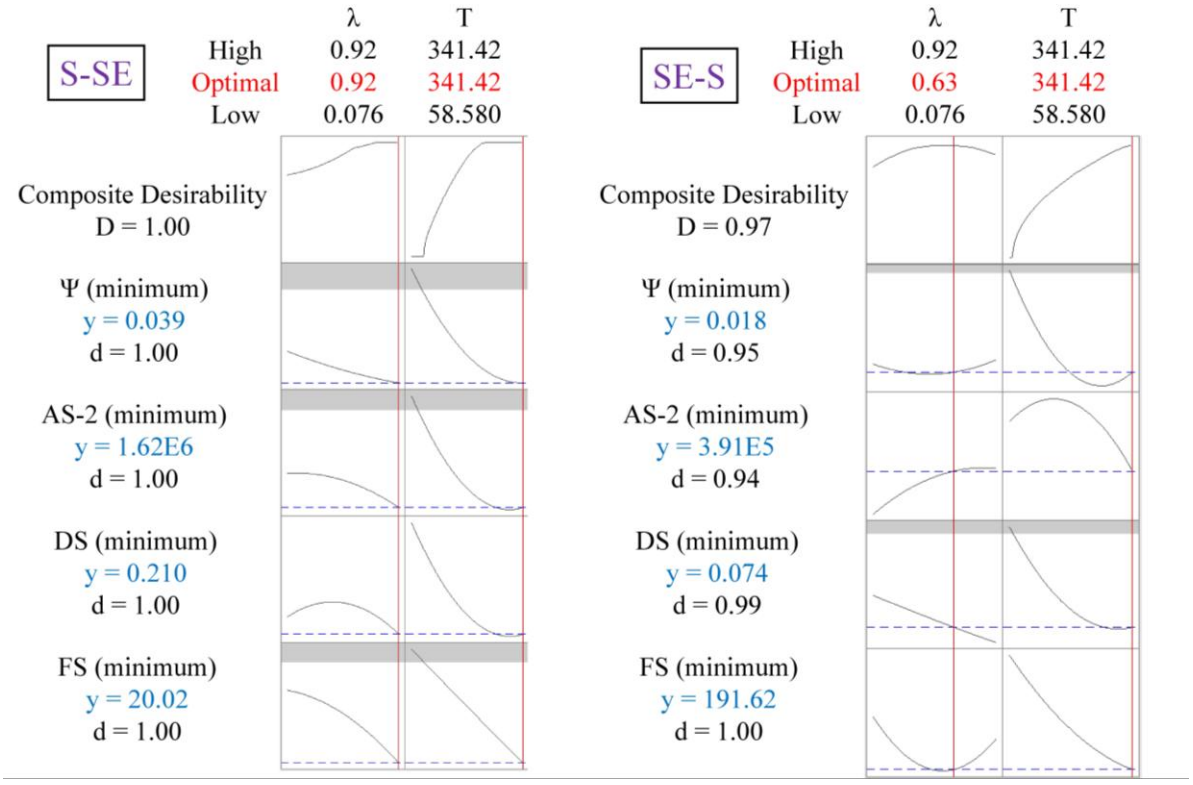

Figure 14 Optimization plots for S-SE and SE-S configurations

4.6 Comparative Analysis of Cushion Configurations

A comparative analysis evaluated four cushion configurations, pure sand (S), optimized sand over EPS-sand mixture (S-SE-F), pure EPS-sand mixture (SE), and optimized EPS-sand mixture over sand (SE-S-F), using optimal thickness ratios from the previous section. These configurations underwent successive impact tests under identical conditions. Figure 15 presents a radar plot of normalized performance across seven parameters: impact force (F_1), transmitted load (F_2), reaction force (FS), penetration depth (PD), displacement (DS), acceleration (AS-2), and global tension damage index (Ψ), with the energy dissipation factor (F_2/F_1 ratio) also considered. Normalization scaled each parameter from 0 (lowest value) to 1 (highest) based on the range across configurations, highlighting relative performance differences.

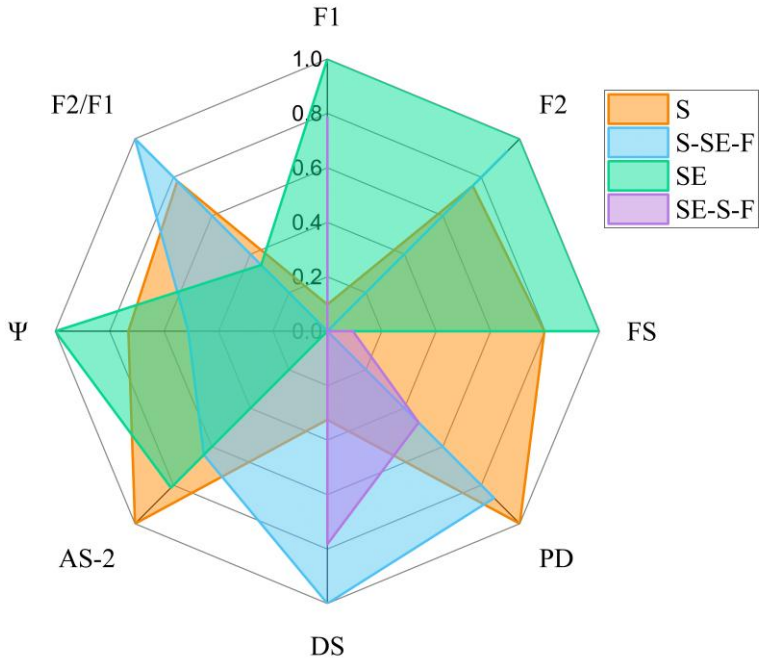

Figure 15 Radar plot comparing normalized performance of four cushion configurations (S, S-SE-F, SE, SE-S-F)

The analysis revealed distinct performance profiles. The SE configuration excelled in minimizing PD and DS, reflecting its ability to absorb and distribute energy, reducing deformation. The S-SE-F configuration outperformed others in reducing F_1 and FS, due to the sand top layer's initial cushioning and the EPS-sand

mixture's subsequent energy dissipation. The SE-S-F configuration showed the most balanced performance, minimizing F_2, AS-2, F_2/F_1 ratio, and Ψ, indicating superior energy dissipation and structural protection. This results from the EPS-sand mixture absorbing impact energy and the sand layer distributing load effectively, lowering transmitted forces and structural damage. The S configuration, while a baseline, was consistently outperformed by optimized designs, underscoring the benefits of material optimization and layering.

Tension damage in the reinforced concrete (RC) slab was analyzed to assess protective capabilities (Figure 16). Optimized layered configurations significantly reduced the global tension damage index (Ψ) compared to monolithic cushions: SE-S-F by 84.3%, S-SE-F by 41.2%, and S by 22.6%, relative to SE (Ψ values: SE = 0.0468, S = 0.0362, S-SE-F = 0.0275, SE-S-F = 0.0074). Crack widths, calculated per EN-1992 (British Standards Institution, 2004) and detailed in Wang et al. (Wang et al., 2024), were 0.0842 mm for SE, 0.0256 mm for S, 0.0125 mm for S-SE-F, and 0.0065 mm for SE-S-F, corresponding to reductions of 69.6%, 85.2%, and 92.3%, respectively, compared to SE. These values meet EN-1992 limits, confirming structural integrity. SE and S showed centralized high-damage zones with radial cracking due to concentrated tensile stresses, with SE exhibiting the most severe damage. S-SE-F displayed more distributed damage with a mix of radial and flexural cracking, while SE-S-F, with the lowest damage, showed minimal flexural cracking along bending zones, reflecting effective load distribution. The dominant failure mechanism in SE and S was radial cracking from localized stress concentration, whereas SE-S-F and S-SE-F shifted to predominantly flexural cracking, as layered designs spread loads more evenly, reducing stress concentrations. SE-S-F's superior performance stems from the EPS-sand mixture's energy absorption and the sand layer's load distribution, while S-SE-F benefits from initial sand cushioning and subsequent EPS-sand dissipation. The SE configuration, despite strong deformation resistance, exhibited the highest tension damage due to less optimal load distribution across the RC slab surface.

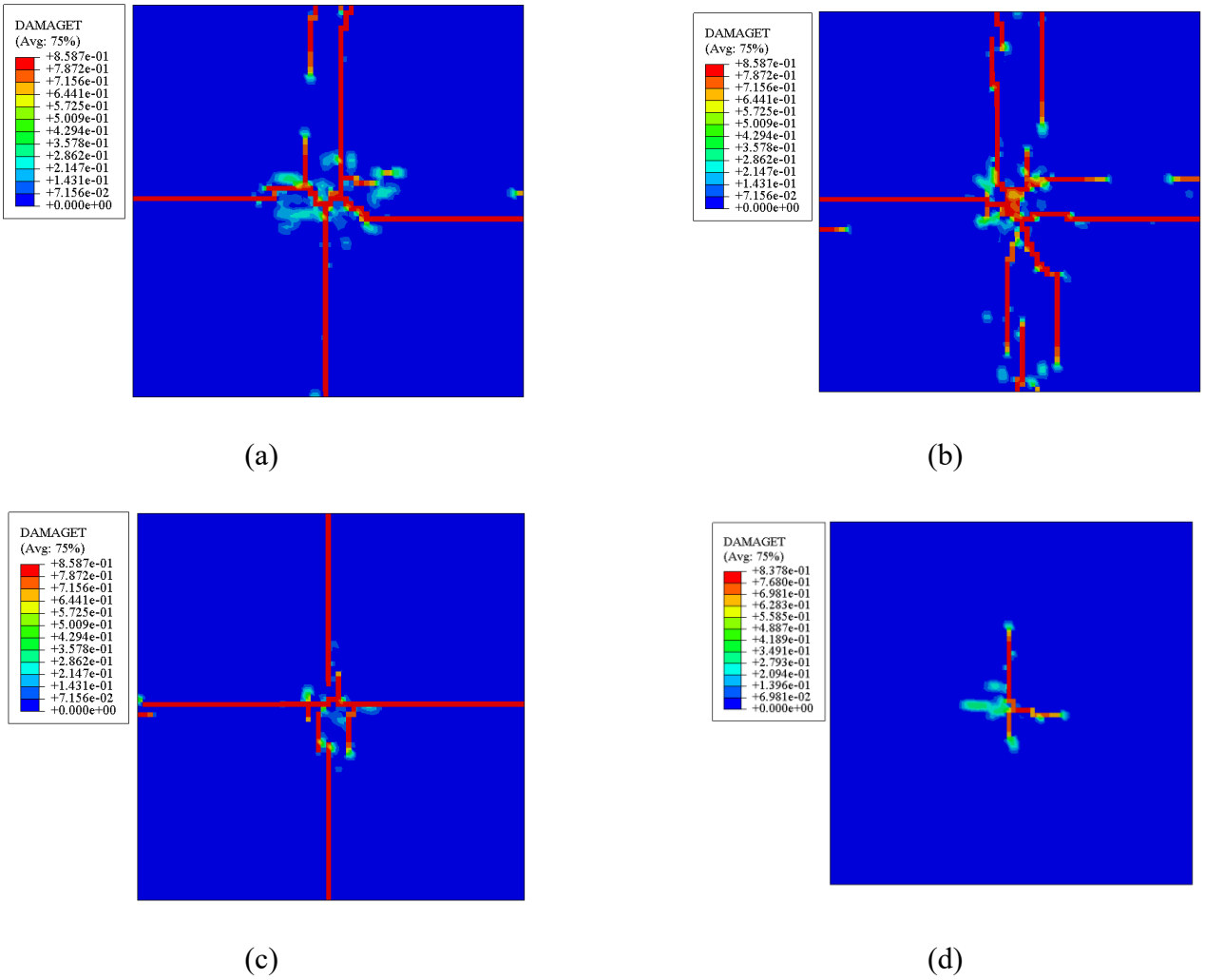

Figure 16 Tensile damage of RC slab for cushion configurations: (a) S, (b) SE, (c) S-SE-F, and (d) SE-S-F.

Future research could explore energy dissipation pathways within layered structures via micro-scale analysis, assess long-term durability under varied environmental conditions and repeated impacts, and investigate the relationship between cushion deformation and load distribution to further enhance cushion designs for rockfall protection.

5 Conclusion

This study advances rockfall mitigation strategies through a comprehensive investigation of EPS bead-sand composite cushions, integrating experimental methodologies, statistical optimization, and numerical

simulations to yield novel insights into cushioning system design for rockfall protection structures. The key findings and contributions are summarized as follows:

1. Optimal EPS-Sand Ratio: Through Orthogonal Experimental Design (OED) and Response Surface Methodology (RSM), an optimal EPS bead content of 38.79% by volume was identified within the 30–40% range, achieving a critical balance between energy absorption and load distribution. This ratio enhances the cushion's protective efficacy by optimizing compressibility and structural stability under impact loads.
2. Superiority of Layered Configurations: Layered cushion configurations, particularly the SE-S-F (EPS-sand mixture over pure sand) design, significantly outperformed monolithic cushions. The SE-S-F configuration achieved a 79.7% reduction in RC slab tension damage (global tension damage index, Ψ) compared to traditional sand cushions (S) (Ψ values: S = 0.0362, SE-S-F = 0.0074) and an 84.3% reduction compared to the pure EPS-sand mixture (SE) (Ψ = 0.0468). Additionally, SE-S-F reduced crack widths by 92.3% relative to SE (crack widths: SE = 0.0842 mm, SE-S-F = 0.0065 mm), while S-SE-F achieved a 41.2% reduction in Ψ and an 85.2% reduction in crack width compared to SE, demonstrating substantial improvements in structural protection.
3. Multifaceted Performance Enhancement: The optimized EPS-sand mixtures and layered configurations exhibited significant improvements across multiple performance indicators. The SE-S-F design excelled in minimizing transmitted forces (F2), accelerations (AS-2), the energy dissipation factor (F2/F1 ratio), and global tension damage (Ψ), while shifting failure mechanisms from radial to flexural cracking due to effective load distribution. The S-SE-F configuration notably reduced impact forces (F1) and reaction forces (FS), benefiting from the sand layer's initial cushioning and the EPS-sand mixture's energy dissipation. These enhancements highlight the potential for more resilient and efficient rockfall protection systems.
4. Sustainability and Circular Economy Contributions: By repurposing waste EPS beads, this research promotes sustainable construction practices and aligns with circular economy principles, offering an

environmentally conscious solution to rockfall mitigation while addressing EPS waste management challenges.

These findings have significant implications for the design and implementation of rockfall protection structures, enabling the development of lighter, more effective, and sustainable systems that enhance safety and reduce costs in mountainous regions and along transportation corridors. However, several limitations must be acknowledged. The study maintained the cushion's moisture content at the Optimum Moisture Content (OMC), without exploring the effects of varying moisture levels on energy absorption and load distribution. It focused on regular rock shapes (cube, sphere, cone) and normal impacts, excluding irregular rocks, oblique collisions, and detailed analyses of rotation, impact area, or penetration depth. The numerical model simplified the EPS-sand mixture as a homogeneous material, potentially overlooking micro-scale interactions between EPS beads and sand. Additionally, the use of EPS beads with a single size range (3–5 mm) and assumed uniform distribution limited the investigation of bead size or distribution effects on stiffness and energy absorption, as noted by Edinçliler and Özer (Edinçliler and Özer, 2014). The experimental setup used only two accelerometers, restricting the capture of a detailed acceleration profile across the RC slab, and the effects of boundary conditions on impact response were not explicitly analyzed.

Future research should investigate the influence of varying moisture levels, irregular rock shapes, oblique impacts, and boundary conditions on cushion performance. Exploring the effects of different EPS bead sizes and distributions, as well as long-term durability under diverse environmental conditions, would further enhance the applicability of these findings. Advanced numerical models, such as the discrete element method for simulating EPS beads, and the deployment of additional sensors for a comprehensive acceleration profile could provide deeper insights. Full-scale field trials, life-cycle assessments, and further material innovations in rockfall protection would also offer valuable perspectives on the real-world performance and sustainability of these systems.

Acknowledgements

This work was supported by the Science and Education Joint Foundation of Sichuan Province (Grant No. 2024NSFSC1952), the National Natural Science Foundation of China (Grant No. 42207232).

REFERENCES

American Society for Testing and Materials, 2021. ASTM D698 - 12: Standard Test Methods for Laboratory Compaction Characteristics of Soil Using Standard Effort (12,400 ft-lbf/ft 3 (600 kN-m/m 3)) 1. ASTM Int. D698 − 12, 7. https://doi.org/10.1520/D0698-12R21.

Arellano, D., Stark, T.D., Horvath, J.S., Leshchinsky, D., 2011. Guidelines for geofoam applications in slope stability projects. Preliminary Draft Final Rep. NCHRP Proj. No. 24-11 02.

ASTM, C., 2006. Standard test method for sieve analysis of fine and coarse aggregates, ASTM C136-06.

ASTM Committee D-18 on Soil and Rock, 2011. Standard test methods for one-dimensional consolidation properties of soils using incremental loading, ASTM International.

ASTM Committee D-18 on Soil and Rock, 2009. Standard Test Methods for Laboratory Compaction Characteristics of Soil Using Modified Effort (56,000 Ft-Lbf/Ft3 (2,700 KN-M/M3)) 1, ASTM international, 2009.

ASTM Committee D-18 on Soil and Rock, 2006. Standard Test Method for Permeability of Granular Soils (constant Head), ASTM international.

Bathurst, R.J., Zarnani, S., Gaskin, A., 2007. Shaking table testing of geofoam seismic buffers. Soil Dyn. Earthq. Eng. 27, 324–332. https://doi.org/10.1016/j.soildyn.2006.08.003

British Standards Institution, 2004. Eurocode 2: Design of Concrete Structures: Part 1-1: General Rules and Rules for Buildings, British Standards Institution.

Budetta, P., 2004. Assessment of rockfall risk along roads. Nat. Hazards Earth Syst. Sci. 4, 71–81. https://doi.org/10.5194/nhess-4-71-2004

Chikatamarla, R., 2007. Optimisation of cushion materials for rockfall protection galleries.

Deshmukh, R., Iyer, S., Bhangare, P., 2022. Geotechnical characterization of Expanded polystyrene (EPS) beads

with industrial waste and its utilization in flexible pavement. Mater. Today Proc. 61, 187–196. https://doi.org/10.1016/j.matpr.2021.07.462

Edinçliler, A., Özer, A.T., 2014. Effects of EPS bead inclusions on stress-strain behaviour of sand. Geosynth. Int. 21, 89–102. https://doi.org/10.1680/gein.14.00001

El-Sherbiny, R.M., Ramadan, S.H., El-Khouly, M.A., 2018. Dynamic properties of sand-EPS bead mixtures. Geosynth. Int. 25, 456–470. https://doi.org/10.1680/jgein.18.00021

Gao, H., Liu, J., Liu, H., 2011. Geotechnical properties of EPS composite soil. Int. J. Geotech. Eng. 5, 69–77. https://doi.org/10.3328/IJGE.2011.05.01.69-77

Hassan, W., Alshameri, B., Jamil, S.M., Maqsood, Z., Haider, A., Shahzad, A., 2023a. Incorporating potassium-rich waste material in a sustainable way to stabilize dispersive clay: A novel practical approach for the construction industry. Constr. Build. Mater. 400, 132717. https://doi.org/10.1016/j.conbuildmat.2023.132717

Hassan, W., Alshameri, B., Nawaz, M.N., Qamar, S.U., 2022. Experimental study on shear strength behavior and numerical study on geosynthetic-reinforced cohesive soil slope. Innov. Infrastruct. Solut. 7, 1–18. https://doi.org/10.1007/s41062-022-00945-2

Hassan, W., Farooq, K., Mujtaba, H., Alshameri, B., Shahzad, A., Nawaz, M.N., Azab, M., 2023b. Experimental investigation of mechanical behavior of geosynthetics in different soil plasticity indexes. Transp. Geotech. 39, 100935. https://doi.org/10.1016/j.trgeo.2023.100935

Horvath, J.S., 2008. Seismic Lateral Earth Pressure Reduction on Earth-Retaining Structures Using Geofoams, in: Geotechnical Earthquake Engineering and Soil Dynamics IV. American Society of Civil Engineers, pp. 1–10. https://doi.org/10.1061/40975(318)155

Jin, Y., Yu, Z., Liao, L., Zhang, L., Luo, L., 2024. The buffering performance of a flexible buffer-sand layer composite cushion used for rockfall shed: experimental and numerical investigation. Landslides 21, 1003–

1022. https://doi.org/10.1007/s10346-023-02196-3

Kishi, N., Konno, H., Ikeda, K., Matsuoka, K.G., 2002. Prototype impact tests on ultimate impact resistance of PC rock-sheds. Int. J. Impact Eng. 27, 969–985. https://doi.org/10.1016/S0734-743X(02)00019-2

Klose, M., Damm, B., Terhorst, B., 2015. Landslide cost modeling for transportation infrastructures: a methodological approach. Landslides 12, 321–334. https://doi.org/10.1007/s10346-014-0481-1

Kurihashi, Y., Kogure, N., Nitta, S.I., Komuro, M., 2020. Experimental Study on Impact Absorption Capacity of Various Expanded Materials for Rock Shed. Shock Vib. 2020. https://doi.org/10.1155/2020/7412456

Lambert, S., Bourrier, F., 2013. Design of rockfall protection embankments: A review. Eng. Geol. 154, 77–88. https://doi.org/10.1016/j.enggeo.2012.12.012

Lambert, S., Gotteland, P., Nicot, F., 2009. Experimental study of the impact response of geocells as components of rockfall protection embankments. Nat. Hazards Earth Syst. Sci. 9, 459–467. https://doi.org/10.5194/nhess-9-459-2009

Lan, H., Martin, C.D., Zhou, C., Lim, C.H., 2010. Rockfall hazard analysis using LiDAR and spatial modeling. Geomorphology 118, 213–223. https://doi.org/10.1016/j.geomorph.2010.01.002

Liu, H. long, Deng, A., Chu, J., 2006. Effect of different mixing ratios of polystyrene pre-puff beads and cement on the mechanical behaviour of lightweight fill. Geotext. Geomembranes 24, 331–338. https://doi.org/10.1016/j.geotexmem.2006.05.002

Loew, S., Hantz, D., Gerber, W., 2022. Rockfall Causes and Transport Mechanisms - A Review, in: Treatise on Geomorphology. Academic Press, pp. 137–168. https://doi.org/10.1016/B978-0-12-818234-5.00066-3

Meree, H., Wang, D., Yan, S., 2023a. Numerical and Theoretical Study of Rockfall Impact on Shed with Composite Sand-Airbag Cushion Materials. Environ. Earth Sci. 82, 432. https://doi.org/doi.org/10.1007/s12665-023-11132-6

Meree, H., Wang, D., Yan, S., Li, M., Lu, S., Lovati, M., Liu, F., 2024. Dynamic response of rock sheds to successive rockfall impacts using lightweight expanded clay aggregate (LECA) cushions: An experimental and numerical study. Int. J. Impact Eng. 193, 105043. https://doi.org/10.1016/j.ijimpeng.2024.105043

Meree, H., Yan, S., Wang, D., Xiang, B., 2023b. A Numerical Study on the performance of Traditional Concrete and Three-Dimensional Printed Concrete Dams under the Boulder Impact, in: International Association for Engineering Geology and the Environment. Singapore: Springer Nature Singapore, pp. 229–240. https://doi.org/doi.org/10.1007/978-981-99-9069-6_16

Meree, H., Yan, S. xing, Wang, D. po, Bi, Y. zhang, 2023c. Behavior of traditional concrete dams and three-dimensional printed concrete dams under the debris flow impact. J. Mt. Sci. 20, 3703–3717. https://doi.org/10.1007/s11629-023-8059-9

Ojuri, O.O., Ademola, S.A., 2016. Compaction and Strength Characteristics of Modified Waste Expanded Polystyrene (EPS) Mixed with a Standard Sand. Geo-China 2, 85–92. https://doi.org/10.1061/9780784480014.011

Savi, S., Comiti, F., Strecker, M.R., 2021. Pronounced increase in slope instability linked to global warming: A case study from the eastern European Alps. Earth Surf. Process. Landforms 46, 1328–1347. https://doi.org/10.1002/esp.5100

Stark, T.D., 2004. Guideline and recommended standard for geofoam applications in highway embankments. Transp. Res. Board 529.

Su, Y., Cui, Y., Ng, C.W.W., Choi, C.E., Kwan, J.S.H., 2019. Effects of particle size and cushioning thickness on the performance of rock-filled gabions used in protection against boulder impact. Can. Geotech. J. 56, 198–207. https://doi.org/10.1139/cgj-2017-0370

Sun, J., Chu, Z., Liu, Y., Luo, W., Wang, M., 2016. Performance of Used Tire Cushion Layer under Rockfall Impact. Shock Vib. 2016. https://doi.org/10.1155/2016/8760592

Tamut, T., Prabhu, R., Venkataramana, K., Yaragal, S.C., 2014. Partial replacement of coarse aggregates by expanded polystyrene beads in concrete. Int. J. Res. Eng. Technol. 3, 238–241. https://doi.org/doi.org/10 .15623/ijret.2014.0302040.

Volkwein, A., Schellenberg, K., Labiouse, V., Agliardi, F., Berger, F., Bourrier, F., Dorren, L.K.A., Gerber, W., Jaboyedoff, M., 2011. Rockfall characterisation and structural protection - A review. Nat. Hazards Earth Syst. Sci. 11, 2617–2651. https://doi.org/10.5194/nhess-11-2617-2011

Wang, D., Bi, Y.Z., Zhou, L., Chen, H., Zhou, R., Lovati, M., 2022. Experimental study on physical model of waste tennis ball-sand composite shed cushion under rockfall impact. Bull. Eng. Geol. Environ. https://doi.org/10.1007/s10064-022-02643-w

Wang, D., Meree, H., Li, H., Yan, S., 2024. Method for Predicting Damage Probability of Shed Tunnel Structures Under Rolling Stone Random Impact Events. 202411587645.X.

Yamada, S., Nagasaka, Y., Nishida, N., Shiroi, A., 1989. Light soil mixture with small pieces of expanded polystyrol and sand. Soil Mech. Found. Eng. 37, 25–30.

Yan, S., Wang, Y., Wang, D., He, S., 2022. Application of EPS geofoam in rockfall galleries: Insights from large-scale experiments and FDEM simulations. Geotext. Geomembranes 50, 677–693. https://doi.org/10.1016/j.geotexmem.2022.03.009

Yu, B., Zhou, X., Tang, J., Zhang, Yujin, Zhang, Yuefeng, 2024. Impact resistance performance and optimization of the sand-EPE composite cushion in rock sheds. J. Mt. Sci. 21, 676–689. https://doi.org/10.1007/s11629-023-8403-0

Zhao, P., Xie, L., He, B., Zhang, Y., 2018a. Experimental study of rock-sheds constructed with PE fibres and composite cushion against rockfall impacts. Eng. Struct. 177, 175–189. https://doi.org/10.1016/j.engstruct.2018.09.073

Zhao, P., Xie, L., Li, L., Liu, Q., Yuan, S., 2018b. Large-scale rockfall impact experiments on a RC rock-shed

with a newly proposed cushion layer composed of sand and EPE. Eng. Struct. 175, 386–398. https://doi.org/10.1016/j.engstruct.2018.08.046